UNIVERSITI PUTRA MALAYSIA

PREPARATION AND CHARACTERISATION OF DIELECTRIC PYROCHLORES IN THE Bi_2O_3-MgO-M_2O_5 (M = Ta AND Nb) TERNARY SYSTEMS

TAN PHEI YI

FS 2015 43

PREPARATION AND CHARACTERISATION OF DIELECTRIC PYROCHLORES IN THE Bi_2O_3-MgO-M_2O_5 (M = Ta AND Nb) TERNARY SYSTEMS

By

TAN PHEI YI

Thesis Submitted to the School of Graduate Studies, Universiti Putra Malaysia, in Fulfilment of the Requirements for the Degree of Doctor of Philosophy

June 2015

COPYRIGHT

Abstract of thesis presented to the Senate of Universiti Putra Malaysia in fulfilment of the requirement for the degree of Doctor of Philosophy

PREPARATION AND CHARACTERISATION OF DIELECTRIC PYROCHLORES IN THE Bi_2O_3-MgO-M_2O_5 (M = Ta AND Nb) TERNARY SYSTEMS

By

TAN PHEI YI

June 2015

Chairman: Tan Kar Ban, PhD
Faculty: Science

A detailed and comprehensive investigation of synthesis and characterisation of the pyrochlores in the Bi_2O_3-MgO-Nb_2O_5 (BMN) and Bi_2O_3-MgO-Ta_2O_5 (BMT) ternary systems was presented. The structural flexibility and variable stoichiometry of these pyrochlore systems had given rise to many interesting properties. The excellent dielectric properties, e.g. low dielectric losses and high dielectric constants had rendered BMN and BMT pyrochlores as potential dielectric applications. Phase pure cubic pyrochlores in both BMN and BMT systems were successfully prepared using conventional solid-state method. As with phase diagram study, phase pure cubic pyrochlores in the Bi_2O_3-MgO-Nb_2O_5 system were found to form in a broad solution area whose compositions with bismuth content between 41.88 mole % and 44.50 mole %. The solid solution area was represented by an overall general formula of $Bi_{3.36+x}Mg_{1.92-y}Nb_{2.72-x+y}O_{13.76-x+(3/2)y}$, which used two variables with the associated limits of $-0.01 \leq x \leq 0.20$ and $0.00 \leq y \leq 0.16$, respectively. On the other hand, pyrochlores in the Bi_2O_3-MgO-Ta_2O_5 system formed a relatively larger subsolidus solution area than that of the BMN system with the overall general formula $Bi_{3.56-x}Mg_{1.96-y}Ta_{2.48+x+y}O_{13.50+x+(3/2)y}$ ($0.00 \leq x \leq 0.32$ and $0.00 \leq y \leq 0.20$).

Both BMN and BMT cubic pyrochlores were found to be thermally stable over a wide range of temperatures, i.e. 30 - 1000 °C. Selected BMN and BMT pyrochlores were characterised by AC impedance spectroscopy and these materials were found to exhibit excellent dielectric properties. High dielectric constants, ε', low dielectric losses, tan δ in the order of 10^{-4} - 10^{-3} were recorded for BMN and BMT pyrochlores whose ε' values were in the range of 167 - 204 and 70 - 85, respectively at temperature of 30 °C and frequency of 1 MHz. Both pyrochlores required high activation energies, Ea > 1.0 eV for their electrical conduction. The high activation energy suggesting that these materials were typical dielectric materials, which their conduction mechanism were governed by the hopping electronic type. Meanwhile, relaxor behaviour was observed for both systems in a

low temperature range of 10 K - 320 K. The electrical data at low temperature range could be accurately fitted with different types of equivalent circuits, e.g. a parallel resistance-capacitance-constant phase element (R-C-CPE) element in series with a capacitor.

In attempts to improve the electrical performance of the pyrochlore materials, chemical doping using divalent cations such as Ni^{2+}, Cd^{2+} and Zn^{2+} cations was performed. Different solid solution limits were obtained and the results showed that dielectric constants and dielectric losses of divalent cations doped solid solutions did not vary significantly with increase of dopants concentration. On the other hand, pentavalent dopant, Nb^{5+} was introduced into BMT cubic pyrochlores using a formula of $Bi_{3.50}Mg_{1.80}Ta_{2.70-x}Nb_xO_{13.80}$ ($0 \leq x \leq 2.70$). It formed a complete substitutional solid solution and the dielectric constants were found to increase with increasing Nb^{5+} concentration. Nb doped BMT pyrochlores exhibited ε’ in the range of 81 - 195 and low dielectric loss of 0.0013 - 0.0059.

Abstrak tesis yang dikemukakan kepada Senat Universiti Putra Malaysia sebagai memenuhi keperluan untuk ijazah Doktor Falsafah

PENYEDIAAN DAN PENCIRIAN BAHAN PIROKLOR DIELEKTRIK DALAM SISTEM TERNARI Bi_2O_3-MgO-M_2O_5 (M = Ta DAN Nb)

Oleh

TAN PHEI YI

June 2015

Pengerusi: Tan Kar Ban, PhD
Fakulti: Sains

Penyelidikan yang terperinci dan menyeluruh bagi sintesis dan pencirian piroklor-piroklor dalam kedua-dua sistem Bi_2O_3-MgO-Nb_2O_5 (BMN) dan Bi_2O_3-MgO-Ta_2O_5 (BMT) telah dijalankan. Terdapat banyak ciri yang menarik ditunjukkan oleh sistem-sistem piroklor berstruktur fleksibel dan berlainan stoikiometri ini. Ciri-ciri dielektrik yang cemerlang, contohnya kehilangan dielektrik yang rendah dan pemalar dielektrik yang tinggi telah membolehkan piroklor-piroklor BMN dan BMT berpotensi dalam aplikasi dielektrik. Fasa tulen piroklor kubus BMN dan BMT telah berjaya disintesis dengan menggunakan kaedah tindak balas keadaan pepejal. Seperti dalam kajian gambarajah fasa, fasa tulen piroklor kubus dalam sistem Bi_2O_3-MgO-Nb_2O_5 menunjukkan kawasan larutan pepejal yang luas di mana komposisinya mengandungi Bi antara 41.88 % mol hingga 44.50 % mol. Kawasan larutan pepejal boleh diwakili oleh formula am, $Bi_{3.36+x}Mg_{1.92-y}Nb_{2.72-x+y}O_{13.76-x+(3/2)y}$ di mana dua pembolehubah yang digunakan mempunyai had $-0.01 \leq x \leq 0.20$ dan $0.00 \leq y \leq 0.16$. Sebaliknya, Bi_2O_3-MgO-Ta_2O_5 membentuk kawasan larutan piroklor kubus yang lebih luas daripada sistem BMN dengan formula keseluruhannya $Bi_{3.56-x}Mg_{1.96-y}Ta_{2.48+x+y}O_{13.50+x+(3/2)y}$ ($0.00 \leq x \leq 0.32$ dan $0.00 \leq y \leq 0.20$).

Kedua-dua piroklor kubus BMN dan BMT menunjukkan kestabilan terma dalam julat suhu 30 - 1000 °C. Piroklor-piroklor BMN dan BMT yang terpilih telah dikaji dengan menggunakan spektroskopi AC impedans dan bahan-bahan ini menunjukkan ciri-ciri dielektrik yang bagus. Pemalar dielektrik yang tinggi dan kehilangan dielektrik yang rendah iaitu pada julat 10^{-4} -10^{-3} telah dicatatkan bagi piroklor-piroklor BMN dan BMT di mana nilai ε' bagi piroklor BMN dan BMT masing-masing dalam lingkungan 167 - 204 dan 70 - 85 pada suhu 30 °C dan frekuensi 1 MHz. Kedua-dua piroklor memerlukan tenaga pengaktifan yang tinggi, Ea > 1.0 eV untuk konduksi elektrik. Tenaga pengaktifan yang tinggi menunjukkan bahawa bahan-bahan ini adalah bahan dielektrik dan mekanisma konduksinya melibatkan lompatan elektron-elektron dalam bahan tersebut. Sementara itu, sifat *relaxor* dapat diperhati bagi kedua-dua sistem dalam lingkungan suhu yang rendah iaitu 10 K - 320 K. Data-data elektrik pada suhu rendah boleh dimuatkan dengan tepat pada litar setara yang berbeza, contohnya susunan selari rintangan-kapasitanelemen fasa berterusan (R-C-CPE) ke dalam susunan siri yang mempunyai satu kapasitor.

Dalam usaha untuk meningkatkan prestasi elektrik atas bahan-bahan piroklor, pendopan kimia dengan menggunakan kation divalen seperti Ni^{2+}, Cd^{2+} dan Zn^{2+} telah dibuat. Larutan pepejal dengan had yang berbeza telah diperolehi dan menunjukkan bahawa tiada perubahan yang ketara dalam pemalar dielektrik dan kehilangan dielektrik apabila bahan dop ditambahkan ke dalam larutan pepejal kation divalen. Selain daripada itu, dopan pentavalen, Nb^{5+} didopkan ke dalam piroklor BMT dengan menggunakan formula $Bi_{3.50}Mg_{1.80}Ta_{2.70-x}Nb_xO_{13.80}$ ($0 \leq x \leq 2.70$). Ia membentuk satu larutan pepejal gantian yang lengkap dan didapati bahawa nilai pemalar dielektriknya meningkat dengan pertambahan kepekatan Nb^{5+}. Piroklor BMT dengan dopan Nb menunjukkan nilai ε' dalam lingkungan 81 - 195 dan mempunyai kehilangan dielectrik yang bernilai 0.0013 - 0.0059.

ACKNOWLEDGEMENTS

It would not have been possible to complete my dissertation without the helps and supports from the kind people around me.

First and foremost, I would like to express my deepest gratitude to my supervisor, Dr. Tan Kar Ban for his patience, motivation, enthusiasm, and immense knowledge. His guidance and encouragement had helped me tremendously throughout my study. I would like to extend my sincere appreciation to Dr. Khaw Chwin Chieh, Professor Dr. Zulkarnain Zainal and Dr. Chen Soo Kien for their meticulous comments, invaluable advice and suggestions in this research work.

My deepest appreciation also dedicated to Professor Dr. A. R. West for the three-month research attachment sponsorship at the Department of Materials Science and Engineering, University of Sheffield. I have greatly benefited for his insightful comments and suggestions. Besides, I am grateful for the assistance and guidance given by Dr. Liu Yang and Dr. Nik Reeves-McLaren in equivalent circuit analysis and XRD analysis. Without their persistent helps, it would not have a fruitful attachment.

I would like to thank the staff of UPM Chemistry Department of UPM especially Madam Zaidina Mohd Daud (XRD), Madam Rusnani Amirudin (IR), Madam Nor Azlina Shari (DTA, TGA) and Madam Nurhidayu Jamaludin (ICP-OES) for their technical assistance and guidance in data collection. My appreciation also goes to all staff in Electron Microscopy Unit, UPM.

In my daily work, I have been blessed with a friendly and cheerful group of fellow lab mates and friends. I would like to thank to Ms. Chon Mun Ping and Dr. Ch’ng Sook Keng for their kindness and continuous support. Not to be forgotten are Mr. Ong Poh Shing, Mr. Wong Yong Chen, Mr. Chuah You Jian, Ms. Chia Chew Theng, Ms. Yew Sook Yan and Mr. Lim Yee Seng for their endless support, laughter and joy all the way through.

The financial supports from the Ministry of Science, Technology and Innovation through National Science Fellowship (NSF) scholarship and Ministry of Higher Education, Malaysia via Fundamental Research Grant Scheme (FRGS) are gratefully acknowledged. My appreciation also express to Graduate School of Studies, UPM via financial aid to my attachment at the University of Sheffield, UK.

Last but not least, my deepest gratitude extended to my beloved family members for their love and spiritual support throughout my life.

This thesis was submitted to the Senate of Universiti Putra Malaysia and has been accepted as fulfilment of the requirement for the degree of Doctor of Philosophy. The members of the Supervisory Committee were as follows:

Tan Kar Ban, Ph.D
Lecturer
Faculty of Science
Universiti Putra Malaysia
(Chairperson)

Zulkarnain Zainal, Ph.D
Professor
Faculty of Science
Universiti Putra Malaysia
(Member)

Chen Soo Kien, Ph. D
Associate Professor
Faculty of Science
Universiti Putra Malaysia
(Member)

Khaw Chwin Chieh, Ph.D
Assistant Professor
Lee Kong Chian Faculty of Engineering and Science
Universiti Tunku Abdul Rahman
(Member)

Bujang Bin Kim Huat, PhD
Professor and Dean
School of Graduate Studies
Universiti Putra Malaysia

Date:

Declaration by graduate student

I hereby confirm that:

- this thesis is my original work;
- quotations, illustrations and citations which have been duly referenced;
- this thesis has not been submitted previously or concurrently for any other degree at any other institutions;
- intellectual property from the thesis and copyright of thesis are fully-owned by Universiti Putra Malaysia, as according to the Universiti Putra Malaysia (Research) Rules 2012;
- written permission must be obtained from supervisor and the office of Deputy Vice-Chancellor (Research and Innovation) before thesis is published (in the form of written, printed or in electronic form) including books, journals, modules, proceedings, popular writing, seminar papers, manuscripts, posters, reports, lecture notes, learning modules or any other materials as stated in the Universiti Putra Malaysia (Research) Rules 2012;
- there is no plagiarism or data falsification/ fabrication in the thesis, and scholarly integrity is upheld as according to the Universiti Putra Malaysia (Graduate Studies) Rules 2003 (Revision 2012-2013) and the Universiti Putra Malaysia (Research) Rules 2012. The thesis has undergone plagiarism detection software.

Signature:____________________ Date:______________________

Name and Matric No.: Tan Phei Yi (GS24179)

Declaration by Members of Supervisory Committee

This is to confirm that:

- the research conducted and the writing of this thesis was under our supervision;
- supervision responsibilities as stated in the Universiti Putra Malaysia (Graduate Studies) Rules 2003 (Revision 2012-2013) are adhered to.

Signature : ________________________
Name of Chairman of
Supervisory Committee : Dr. Tan Kar Ban

Signature : ________________________
Name of Chairman of
Supervisory Committee : Prof. Dr. Zulkarnain Zainal

Signature : ________________________
Name of Chairman of
Supervisory Committee : Dr. Chen Soo Kien

Signature : ________________________
Name of Chairman of
Supervisory Committee : Dr. Khaw Chwin Chieh

TABLE OF CONTENTS

Page

ABSTRACT **i**

ABSTRAK **iii**

ACKNOWLEDGEMENTS **v**

APPROVAL **vi**

DECLARATION **viii**

LIST OF TABLES **xiii**

LIST OF FIGURES **xvii**

LIST OF ABBREVATION **xxx**

CHAPTER

1. INTRODUCTION **1**
- 1.1. Electroceramic 1
- 1.2. The Properties of Dielectric Materials 1
  - 1.2.1. Polarisability 1
    - 1.2.1.1. Types of Polarisation Mechanism 2
  - 1.2.2. Permittivity 3
  - 1.2.3. Dielectric Loss 4
  - 1.2.4. Temperature Coefficient of Capacitance (TCC) 5
- 1.3. Applications of Dielectric Materials 5
  - 1.3.1. Low Temperature Cofired Ceramic (LTCC) 5
  - 1.3.2. High Frequency Dielectric Ceramic 6
  - 1.3.3. Capacitor 7
  - 1.3.4. Multilayer Ceramic Capacitors (MLCCs) 7
  - 1.3.5. Piezoelectric Ceramics 9
  - 1.3.6. Pyroelectric Ceramics 9
- 1.4. Problem Statements 10
- 1.5. Objectives 10

2. LITERATURE REVIEW **11**
- 2.1. Introduction of Pyrochlore 11
  - 2.1.1. $A_2^{3+}B_2^{4+}O_7$ (3+, 4+) pyrochlores 14
  - 2.1.2. $A_2^{2+}B_2^{5+}O_7$ (2+, 5+) pyrochlores 15
  - 2.1.3. Defect pyrochlores 15
- 2.2. Bi-based Pyrochlores 16
- 2.3. Bismuth Zinc Niobate (BZN) Pyrochlore 17
- 2.4. Bismuth Zinc Tantalate (BZT) Pyrochlore 21
- 2.5. Bismuth Magnesium Niobate (BMN) and Bismuth Magnesium Tantalate (BMT) Pyrochlores 23

3. METHODOLOGY **26**
- 3.1. Sample Preparation 26
  - 3.1.1. BMN and BMT Cubic Pyrochlores 26
  - 3.1.2. Phase Diagrams Study in BMN and BMT Ternary 27
  - 3.1.3. Chemical Doping 27
- 3.2. Pellet Preparation 27
- 3.3. Characterisation and Analysis 28

3.3.1. X-ray Diffraction (XRD) 28
3.3.2. Scanning Electron Microscopy (SEM) 29
3.3.3. Thermal Analysis - Differential Thermal Analysis (DTA) and Thermogravimetric Analysis TGA 29
3.3.4. Elemental Analysis- Inductively Coupled Plasma-Atomic Emission Spectrosmetry (ICP-OES) 30
3.3.5. Fourier Transform Infrared Spectroscopy (FT-IR) 31
3.3.6. Raman Spectroscopy 31
3.3.7. Electrical Properties 31
3.3.7.1. Fundamental Impedance Techniques 31
3.3.7.2. Impedance Spectroscopy Data Processing 35
3.3.7.3. Equivalent Circuit Analysis 37
3.3.7.4. Experimental Procedure 37

4. RESULTS AND DISCUSSION 39
4.1. Bi_2O_3-MgO-Nb_2O_5 (BMN) Ternary System 39
4.1.1. Introduction 39
4.1.2. Nominal Compositions, $Bi_3Mg_2Nb_3O_{14}$ and $Bi_4Mg_{4/3}Nb_{8/3}O_{14}$ 39
4.1.3. Phase Diagram of Bi_2O_3-MgO-Nb_2O_5 (BMN) Ternary System 44
4.1.3.1. Cubic Pyrochlore Homogeneity Range in the BMN system 51
4.1.3.2. XRD Analysis of Pyrochlore Solid Solutions 56
4.1.3.3. Thermal Analyses 62
4.1.4. Structural Analysis 65
4.1.4.1. FT-IR Spectroscopy and Raman Spectroscopy 65
4.1.4.2. Scanning Electron Microscopy 69
4.1.5. High Temperature Electrical Properties of Phase Pure BMN Pyrochlores 78
4.1.5.1. Cubic Pyrochlore Solid Solutions 78
4.1.5.2. Conclusion 90
4.1.6. Low Temperature Electrical Properties of Phase Pure BMN Pyrochlores 90
4.1.6.1. Introduction 90
4.1.6.2. Experimental Impedance Data 91
4.1.6.3. Interpretation of Impedance Data and Circuit Modelling 97
4.1.6.4. Discussion 103
4.1.6.5. Conclusion 105
4.1.7. Doped BMN Pyrochlores 105
4.1.7.1. Divalent Doped BMN Pyrochlores 106
4.1.7.2. Surface Morphology Study 110
4.1.7.3. Elemental Analysis 117
4.1.7.4. Thermal Analysis 118
4.1.7.5. Electrical Properties 122
4.1.7.6. Conclusion 130
4.2. Bi_2O_3-MgO-Ta_2O_5 (BMT) Ternary System 131
4.2.1. Introduction 131

4.2.2. Phase formation of compositions $Bi_3Mg_2Ta_3O_{14}$ and $Bi_4Mg_{4/3}Ta_{8/3}O_{14}$ 132
4.2.3. Phase Diagram of Bi_2O_3-MgO-Ta_2O_5 (BMT) Ternary System 134
  4.2.3.1. Cubic Pyrochlore Homogeneity Range 142
  4.2.3.2. XRD Analysis of Pyrochlore Solid Solutions 145
  4.2.3.3. Elemental Analysis 155
  4.2.3.4. Thermal Analysis 156
4.2.4. Structural Analysis 160
  4.2.4.1. FT-IR Spectroscopy and Raman Spectroscopy 160
  4.2.4.2. Scanning Electron Microscopy 166
4.2.5. High Temperature Electrical Properties of Phase Pure BMT Pyrochlores 178
  4.2.5.1. Cubic Pyrochlore Solid Solutions 178
  4.2.5.2. Conlcusion 191
4.2.6. Low Temperature Electrical Properties of Phase Pure BMT Pyrochlores 191
  4.2.6.1. Introduction 191
  4.2.6.2. Experimental Impedance Data 192
  4.2.6.3. Interpretation of Impedance Data and Circuit Modelling 199
  4.2.6.4. Discussion 206
  4.2.6.5. Conclusion 207
4.2.7. Doped BMT Pyrochlore Materials 208
  4.2.7.1. Divalent Doped of BMT Pyrochlore 209
    4.2.7.1.1. Surface Morphology Study 213
    4.2.7.1.2. Elemental Analysis 218
    4.2.7.1.3. Thermal Analysis 218
    4.2.7.1.4. Electrical Properties 221
  4.2.7.2. Pentavalent Doped, Nb BMT Pyrochlore 225
    4.2.7.2.1. Surface Morphology Study 227
    4.2.7.2.2. Thermal Analysis 230
    4.2.7.2.3. Elemental Analysis 231
    4.2.7.2.4. Electrical Properties 232
    4.2.7.2.5. Conclusion 236

5. CONCLUSION **237**
5.1. Recommendation for Future Research 238

REFERENCES **239**
APPENDICES **252**
BIODATA OF STUDENT **278**
LIST OF PUBLICATIONS **279**

LIST OF TABLES

Table **Page**

1.1 Today's most important group of microwave ceramics (Wersing, 1991). 6

1.2 Typical ceramic dielectric materials for MLCCs with several EIA specifications (Kishi *et al*., 2003; Khan *et al*., 1987). 9

2.1 Crystal data on $A_2B_2O_6$ defect pyrochlores (Subramanian *et al*., 1983). 15

2.2 Comparison of the dielectric constants in bismuth-based pyrochlores at different frequencies. 25

3.1 Wavelength used in ICP-OES analysis. 30

3.2 Capacitance values and their possible interpretation (Irvine *et al*., 1990). 33

4.1 Indexed X-ray diffraction pattern of $Bi_{3.36}Mg_{1.92}Nb_{2.72}O_{13.76}$ cubic pyrochlore. 42

4.2 Results of phases present in compositions prepared in the Bi_2O_3-MgO-Nb_2O_5 ternary system. 49

4.3 Elemental concentrations of the selected pyrochlore compositions. 56

4.4 IR absorption bands of SS1(x = -0.01, 0.04, 0.09, 0.14, 0.19; y = 0.06, 0.08, 0.10, 0.12, 0.14) solid solution. 66

4.5 IR absorption bands of SS2 (y = 0.04; x = 0.00 - 0.08) solid solution. 67

4.6 Raman active modes of selected cubic pyrochlores. 69

4.7 Calculated grain sizes, crystallite sizes and strains of SS1 (x = -0.01, 0.04, 0.09, 0.14, 0.19; y = 0.06, 0.08, 0.10, 0.12, 0.14) pyrochlores. 74

4.8 Calculated grain sizes, crystallite sizes and strains of SS2 (y = 0.04; x = 0.00 - 0.08) pyrochlores. 74

4.9 Electrical properties of $Bi_{3.36+x}Mg_{1.92-y}Nb_{2.72-x+y}O_{13.76-x+(3/2)y}$ pyrochlores, SS1 (x = -0.01, 0.04, 0.09, 0.14, 0.19; y = 0.06, 0.08, 0.10, 0.12, 0.14) pyrochlores. 83

4.10 Electrical properties of $Bi_{3.36+x}Mg_{1.92-y}Nb_{2.72-x+y}O_{13.76-x+(3/2)y}$ 83 pyrochlores, SS2 (y = 0.04; x = 0.00 - 0.08).

4.11 The temperatures for which the dielectric constant maximum (T_m), dielectric constant maximum (ε'_{max}), diffuseness constant (γ), Curie-Weiss temperature (T_0) and Burns temperature (T_B) at different frequencies. 95

4.12 Fitting data of $Bi_{3.55}Mg_{1.78}Nb_{2.67}O_{13.78}$ from 10 K to 320 K. 100

4.13 Lattice parameters of $(Bi_{3.50}Mg_{0.50})(Mg_{1.30-x}N_xNb_{2.70})O_{13.80}$ (N = Zn and Ni) and $(Bi_{3.50}Mg_{0.50-x}Cd_x)(Mg_{1.30}Nb_{2.70})O_{13.80}$ pyrochlores. 109

4.14 Calculated grain sizes, crystallite sizes and strains of $(Bi_{3.50}Mg_{0.50})(Mg_{1.30-x}N_xNb_{2.70})O_{13.80}$ (N = Zn and Ni) and $(Bi_{3.50}Mg_{0.50-x}Cd_x)(Mg_{1.30}Nb_{2.70})O_{13.80}$ pyrochlores. 111

4.15 Elemental analyses of $(Bi_{3.50}Mg_{0.50})(Mg_{1.30-x}Zn_xNb_{2.70})O_{13.80}$ ($0 \leq x \leq 0.40$) pyrochlores. 117

4.16 Elemental analyses of Cd doped materials in $(Bi_{3.50}Mg_{0.50-x}Cd_x)(Mg_{1.30}Nb_{2.70})O_{13.80}$ ($0.10 \leq x \leq 0.30$) pyrochlores. 118

4.17 Electrical properties of Zn doped BMN pyrochlores using formula $(Bi_{3.50}Mg_{0.50})(Mg_{1.30-x}Zn_xNb_{2.70})O_{13.80}$. 130

4.18 Electrical properties of Cd doped BMN pyrochlores using formula $(Bi_{3.50}Mg_{0.50-x}Cd_x)(Mg_{1.30}Nb_{2.70})O_{13.80}$. 130

4.19 Electrical properties of Ni doped BMN pyrochlores $(Bi_{3.50}Mg_{0.50})(Mg_{1.30-x}Ni_xNb_{2.70})O_{13.80}$. 130

4.20 Results of phases present in compositions prepared in the Bi_2O_3-MgO-Ta_2O_5 ternary system. 139

4.21 Indexed X-ray diffraction pattern for $Bi_{3.56}Mg_{1.96}Ta_{2.48}O_{13.50}$ cubic pyrochlore. 145

4.22 Elemental concentrations of the selected BMT cubic pyrochlores. 155

4.23 The phonon modes in the infrared spectra of $Bi_{3.56-x}Mg_{1.96-y}Ta_{2.48+x+y}O_{13.50+x+(3/2)y}$ pyrochlores, SS3 (x = 0.01, 0.06, 0.11, 0.16, 0.21, 0.26; y = 0.18, 0.16, 0.14, 0.12, 0.10, 0.08). 162

4.24 The phonon modes in the infrared spectra of $Bi_{3.56-x}Mg_{1.96-y}Ta_{2.48+x+y}O_{13.50+x+(3/2)y}$ pyrochlores, SS4 with y = 0.00; $0.00 \leq x \leq 0.32$. 162

4.25 The phonon modes in the infrared spectra of $Bi_{3.56}Mg_{1.96-}$ 163

$_{y}Ta_{2.48+y}O_{13.50+3y/2}$ pyrochlores, SS5 with x = 0.00; 0.00 ≤ y ≤ 0.20.

4.26 Raman active modes of $Bi_{3.56-x}Mg_{1.96-y}Ta_{2.48+x+y}O_{13.50+x+(3/2)y}$ pyrochlores, SS4 with y = 0.00; 0.00 ≤ x ≤ 0.32 pyrochlores. 165

4.27 Raman active modes of SS5, $Bi_{3.56-x}Mg_{1.96-y}Ta_{2.48+x+y}O_{13.50+x+(3/2)y}$ (x = 0.00; 0.00 ≤ y ≤ 0.20) pyrochlores. 166

4.28 Calculated grain sizes, crystallite sizes and strains of $Bi_{3.56-x}Mg_{1.96-y}Ta_{2.48+x+y}O_{13.50+x+(3/2)y}$ pyrochlores, SS3 with x = 0.01, 0.06, 0.11, 0.16, 0.21, 0.26; y = 0.18, 0.16, 0.14, 0.12, 0.10, 0.08. 177

4.29 Calculated grain sizes, crystallite sizes and strains of $Bi_{3.56-x}Mg_{1.96-y}Ta_{2.48+x+y}O_{13.50+x+(3y/2)}$ pyrochlores, SS4 with y = 0.00; 0.00 ≤ x ≤ 0.32. 177

4.30 Calculated grain sizes, crystallite sizes and strains of $Bi_{3.56-x}Mg_{1.96-y}Ta_{2.48+x+y}O_{13.50+x+3y/2}$ pyrochlores, SS5 with x = 0.00; 0.00 ≤ y ≤ 0.20. 178

4.31 Summary of electrical properties of the pyrochlores in $Bi_{3.56-x}Mg_{1.96-y}Ta_{2.48+x+y}O_{13.50+x+(3/2)y}$ (x = 0.01, 0.06, 0.11, 0.16, 0.21, 0.26; y = 0.18, 0.16, 0.14, 0.12, 0.10, 0.08) , SS3. 185

4.32 Summary of electrical properties of $Bi_{3.56-x}Mg_{1.96-y}Ta_{2.48+x+y}O_{13.50+x+(3y/2)}$ (0.00 ≤ x ≤ 0.32; y = 0.00) pyrochlores. 185

4.33 Summary of electrical properties of $Bi_{3.56-x}Mg_{1.96-y}Ta_{2.48+x+y}O_{13.50+x+3y/2}$ (0.00 ≤ y ≤ 0.20; x = 0.00) pyrochlores. 185

4.34 The temperatures for which the dielectric constant maximum (T_m), dielectric constant maximum (ε'_{max}), diffuseness constant (γ), Curie-Weiss temperature (T_0) and Burns temperature (T_B) at different frequencies. 196

4.35 Fitting data of $Bi_{3.30}Mg_{1.88}Ta_{2.82}O_{13.88}$ from 10 K to 320 K. 203

4.36 Lattice parameters of $(Bi_{3.50}Mg_{0.50})(Mg_{1.30-x}M_xTa_{2.70})O_{13.80}$ (M = Zn and Ni) and $(Bi_{3.50}Mg_{0.50-x}Cd_x)(Mg_{1.30}Ta_{2.70})O_{13.80}$ pyrochlores. 212

4.37 Calculated grain sizes, crystallite sizes and strains of $(Bi_{3.50}Mg_{0.50})(Mg_{1.30-x}M_xTa_{2.70}O_{13.80}$ (M = Zn and Ni) and $(Bi_{3.50}Mg_{0.50-x}Cd_x)(Mg_{1.30}Ta_{2.70}O_{13.80}$ pyrochlores. 217

4.38 Elemental analyses of $(Bi_{3.50}Mg_{0.50})(Mg_{1.30-x}Zn_xTa_{2.70}O_{13.80}$ and $(Bi_{3.50}Mg_{0.50-x}Cd_x)(Mg_{1.30}Ta_{2.70}O_{13.80}$ pyrochlores. 218

4.39 Summary of dielectric properties of $(Bi_{3.50}Mg_{0.50})(Mg_{1.30-x}M_xTa_{2.70}O_{13.80}$ (M = Zn and Ni) and $(Bi_{3.50}Mg_{0.50-x}Cd_x)(Mg_{1.30}Ta_{2.70}O_{13.80}$ pyrochlores. 222

4.40 The calculated grain sizes, crystallite sizes and strains of $(Bi_{3.50}Mg_{0.50})(Mg_{1.30}Nb_xTa_{2.70-x})O_{13.80}$ pyrochlores. 227

4.41 Elemental analyses of Zn doped materials in $(Bi_{3.50}Mg_{0.50})(Mg_{1.30}Nb_xTa_{2.70-x})O_{13.80}$ $(0.0 \leq x \leq 2.70)$. 231

4.42 Summary of electrical properties of $(Bi_{3.50}Mg_{0.50})(Mg_{1.30}Nb_xTa_{2.70-x})O_{13.80}$ pyrochlores. 234

LIST OF FIGURES

Figure **Page**

1.1 Electronic polarisation (Nowotny, 1992) 2

1.2 Space charge polarisation (Nowotny, 1992). 2

1.3 Dipole polarisation (Nowotny, 1992). 2

1.4 Ionic (atomic) polarisation (Nowotny, 1992). 3

1.5 (a) A parallel-plate dielectric capacitor in the form of air separated by plates that are connected to a voltage supply, which makes one plate positively charged while the other plate is negatively charged (Chung, 2010). 4

1.5 (b) A parallel-plate capacitor like that in Figure 1.5 (a), except that the air between the two plates is replaced by a dielectric material (i.e. an electrical insulator) (Chung, 2010). 4

1.6 Assembled capacitor and disc capacitor, respectively (Khan *et al*., 1987). 7

1.7 Cut-away view of multilayer ceramic capacitor (Kishi *et al*., 2003). 8

2.1 Pyrochlore structure as derived from a fluorite lattice. The cation positions for one quarter of the unit cell are shown. The shifts of (48*f*) oxygen towards the (8*a*) (Subramanian *et al*., 1983). 12

2.2 (a) and (b) Illustration of the (a) B_2O_6 and (b) A_2O' interpenetrating network in the pyrochlore. (c) The coordination unit of a (puckered) hexagonal bipyramid (AO_6O_2') (Levin *et al*., 2002). 12

2.3 Projection of the pyrochlore structure based on corner shared BO_6 octahedra. The center of the hexagons contained overlapping projection of one A cation and 2 O’ (8b) anions (Subramanian *et al*., 1983). 13

2.4 The ideal pyrochlore $A_2B_2O_7$ or B_2O_6. $O'A_2$ structure type projected along a <110> direction. The B_2O_6 octahedral framework substructure is represented by the open octahedra while the $O'A_2$ tetrahedral framework sub-structure is represented by the solid tetrahedral. The unit cell is shown in projection (Nguyen *et al*., 2007(a)). 13

2.5 The pyrochlore structure as two interpenetrating networks of BO_6 octahedra and A_2O' chains (Subramanian *et al*., 1983). 13

2.6 Possible substitutions at the A and B sites of $A_2^{3+}B_2^{4+}O_7$ pyrochlores (Subramanian *et al*., 1983). 14

2.7 Possible substitutions at the A and B sites of $A_2^{2+}B_2^{5+}O_7$ pyrochlore (Subramanian *et al*., 1983) 15

3.1 Flow chart for sample preparation using conventional solid-state method. 26

3.2 Flow chart of samples preparation and characterisation. 28

3.3 The impedance Z plotted as a planar vector using rectangular and polar coordinates (Macdonald and Johnson, 2005). 32

3.4 (a) Impedance response for equivalent circuits arranged in parallel (Macdonald and Johnson, 2005). 34

3.4 (b) Impedance response for equivalent circuits arranged in series (Macdonald and Johnson, 2005). 34

3.5 A typical equivalent circuit used to analyses impedance spectroscopy data of electroceramics (Sinclair *et al*., 2000). 35

3.6 *Z**, (a), M*, (b), and combined Z'', M'' spectra, (c), for the circuit in Figure 3.5 where R_b = 20 kW, C_b = 60 pF, R_{gb} = 1 M Ω and C_{gb} = 1 nF. Inset in (a) shows the high frequency response in Z* (circled) (Sinclair *et al*., 2000). 36

4.1 XRD patterns of composition $Bi_3Mg_2Nb_3O_{14}$ in sintering temperature range of (a) 950 - 1100 °C; (b) 800 - 925 °C. 40

4.2 XRD patterns of composition $Bi_4Mg_{4/3}Nb_{8/3}O_{14}$ in sintering temperature range of 800 - 1000 °C. 43

4.3 Isothermal regions in Bi_2O_3-MgO-Nb_2O_5 ternary system. 46

4.4 Subsolidus phase diagram of Bi_2O_3-MgO-Nb_2O_5 ternary system. 47

4.5 Partial subsolidus phase diagram of the Bi_2O_3-MgO-Nb_2O_5. 48

4.6 Expanded cubic pyrochlore solid solution area superposed on the compositional grid with x and y as variables in the formula, $Bi_{3.36+x}Mg_{1.92-y}Nb_{2.72-x+y}O_{13.76-x+(3/2)y}$. 52

4.7 Subsolidus cubic pyrochlore area in different Bi_2O_3-M-Nb_2O_5 ternary system (M = MgO, Mn_2O_3, Fe_2O_3, CoO, NiO and ZnO). 54

4.8 Location of subsolidus compositions of $Bi_{3.36+x}Mg_{1.92-y}Nb_{2.72-x+y}O_{13.76-x+(3/2)y}$, SS1 (x = -0.01, 0.04, 0.09, 0.14, 0.19; y = 0.06, 0.08, 0.10, 0.12 and 0.14) in the Bi_2O_3-MgO-Nb_2O_5 ternary 57 system.

4.9 XRD patterns of $Bi_{3.36+x}Mg_{1.92-y}Nb_{2.72-x+y}O_{13.76-x+(3/2)y}$ pyrochlores, SS1 (a) x = -0.01, 0.04, 0.09, 0.14, 0.19, 0.24; y = 0.06, 0.08, 0.10, 0.12 0.14 and 0.16; (b) x = 0.24; y = 0.16. 58

4.10 Location of composition of $Bi_{3.36+x}Mg_{1.92-y}Nb_{2.72-x+y}O_{13.76-x+(3/2)y}$ pyrochlores, SS2 with y = 0.04; x = 0.00, 0.04 and 0.08. 59

4.11 XRD patterns of $Bi_{3.36+x}Mg_{1.92-y}Nb_{2.72-x+y}O_{13.76-x+(3/2)y}$ pyrochlores, SS2 with y = 0.04; x = -0.04, 0.00, 0.04, 0.08 and 0.12. 60

4.12 Variation of lattice parameters of $Bi_{3.36+x}Mg_{1.92-y}Nb_{2.72-x+y}O_{13.76-x+(3/2)y}$ pyrochlores, SS1 with x = -0.01, 0.04, 0.09, 0.14, 0.19; y = 0.06, 0.08, 0.10, 0.12 and 0.14. 61

4.13 Variation of lattice parameters of $Bi_{3.36+x}Mg_{1.92-y}Nb_{2.72-x+y}O_{13.76-x+(3/2)y}$ pyrochlores, SS2 with y = 0.04; x = 0.00, 0.04 and 0.08. 62

4.14 DTA thermograms of $Bi_{3.36+x}Mg_{1.92-y}Nb_{2.72-x+y}O_{13.76-x+(3/2)y}$ pyrochlores, SS1 with x = -0.01, 0.04, 0.09, 0.14, 0.19; y = 0.06, 0.08, 0.10, 0.12 and 0.14. 63

4.15 DTA thermograms of $Bi_{3.36+x}Mg_{1.92-y}Nb_{2.72-x+y}O_{13.76-x+(3/2)y}$ pyrochlores, SS2 with y = 0.04; x = 0.00, 0.04 and 0.08. 63

4.16 TGA thermograms of $Bi_{3.36+x}Mg_{1.92-y}Nb_{2.72-x+y}O_{13.76-x+(3/2)y}$ pyrochlores, SS1 with x = -0.01, 0.04, 0.09, 0.14, 0.19; y = 0.06, 0.08, 0.10, 0.12 and 0.14. 64

4.17 TGA thermograms $Bi_{3.36+x}Mg_{1.92-y}Nb_{2.72-x+y}O_{13.76-x+(3/2)y}$ pyrochlores, SS2 with y = 0.04; x = 0.00, 0.04 and 0.08. 64

4.18 IR spectra of $Bi_{3.36+x}Mg_{1.92-y}Nb_{2.72-x+y}O_{13.76-x+(3/2)y}$ pyrochlores, SS1 with x = -0.01, 0.04, 0.09, 0.14, 0.19; y = 0.06, 0.08, 0.10, 0.12 and 0.14. 65

4.19 IR spectra of $Bi_{3.36+x}Mg_{1.92-y}Nb_{2.72-x+y}O_{13.76-x+(3/2)y}$ pyrochlores, SS2 with y = 0.04; x = 0.00, 0.04 and 0.08. 66

4.20 Raman spectra of selected cubic pyrochlores in solid solution area at ambient temperature. 67

4.21 SEM micrographs, $Bi_{3.36+x}Mg_{1.92-y}Nb_{2.72-x+y}O_{13.76-x+(3/2)y}$ pyrochlores, SS1 with x = -0.01, 0.04, 0.09, 0.14, 0.19; y = 0.06, 0.08, 0.10, 0.12 and 0.14 recorded at magnification of 5 k. 70

4.22 SEM micrographs of $Bi_{3.36+x}Mg_{1.92-y}Nb_{2.72-x+y}O_{13.76-x+(3/2)y}$ pyrochlores. SS2 with y = 0.04; x = 0.00, 0.04 and 0.08. 72

4.23 Williamson-Hall plots of $Bi_{3.36+x}Mg_{1.92-y}Nb_{2.72-x+y}O_{13.76-x+(3/2)y}$ pyrochlores, SS1 with x = -0.01, 0.04, 0.09, 0.14, 0.19; y = 0.06, 0.08, 0.10, 0.12 and 0.14. 75

4.24 Willianson-Hall plots of $Bi_{3.36+x}Mg_{1.92-y}Nb_{2.72-x+y}O_{13.76-x+(3/2)y}$ pyrochlores, SS2 with y = 0.04; x = 0.00, 0.04 and 0.08. 75

4.25 Scherrer equation and Williamson-Hall plots of $Bi_{3.36+x}Mg_{1.92-y}Nb_{2.72-x+y}O_{13.76-x+(3/2)y}$ pyrochlores, SS1 with x = -0.01, 0.04, 0.09, 0.14, 0.19; y = 0.06, 0.08, 0.10, 0.12 and 0.14. 76

4.26 Scherrer equation and Williamson-Hall plots of $Bi_{3.36+x}Mg_{1.92-y}Nb_{2.72-x+y}O_{13.76-x+(3/2)y}$ pyrochlores, SS2 with y = 0.04; x = 0.00, 0.04 and 0.08. 76

4.27 (111) and (222) diffraction planes of $Bi_{3.36+x}Mg_{1.92-y}Nb_{2.72-x+y}O_{13.76-x+(3/2)y}$ pyrochlores, SS1 with x = -0.01, 0.04, 0.09, 0.14, 0.19; y = 0.06, 0.08, 0.10, 0.12 and 0.14. 77

4.28 (111) and (222) diffraction planes of $Bi_{3.36+x}Mg_{1.92-y}Nb_{2.72-x+y}O_{13.76-x+(3/2)y}$ pyrochlores, SS2 with y = 0.04; x = 0.00, 0.04 and 0.08. 77

4.29 Cole-cole plots of $Bi_{3.50}Mg_{1.80}Nb_{2.70}O_{13.80}$ measured at different temperatures. 79

4.30 Combined Z’’ and M’’ spectroscopic plots for cubic pyrochlore, $Bi_{3.50}Mg_{1.80}Nb_{2.70}O_{13.80}$ at temperature 598 °C. 80

4.31 Imaginary part of impedance as a function of frequency for cubic pyrochlore, $Bi_{3.50}Mg_{1.80}Nb_{2.70}O_{13.80}$ at various temperatures. 81

4.32 Conductivity Arrhenius plots of $Bi_{3.36+x}Mg_{1.92-y}Nb_{2.72-x+y}O_{13.76-x+(3/2)y}$ pyrochlores, SS1 with x = -0.01, 0.04, 0.09, 0.14, 0.19; y = 0.06, 0.08, 0.10, 0.12 and 0.14. 82

4.33 Conductivity Arrhenius plots of $Bi_{3.36+x}Mg_{1.92-y}Nb_{2.72-x+y}O_{13.76-x+(3/2)y}$ pyrochlores, SS2 with y = 0.04; x = 0.00, 0.04 and 0.08. 82

4.34 Dielectric constants and dielectric losses of $Bi_{3.36+x}Mg_{1.92-y}Nb_{2.72-x+y}O_{13.76-x+(3/2)y}$ pyrochlores, SS1 with x = -0.01, 0.04, 0.09, 0.14, 0.19; y = 0.06, 0.08, 0.10, 0.12 and 0.14 at room temperature and frequency of 1 MHz. 85

4.35 Dielectric constants and dielectric losses of $Bi_{3.36+x}Mg_{1.92-y}Nb_{2.72-x+y}O_{13.76-x+(3/2)y}$ pyrochlores, SS2 with y = 0.04; x = 0.00, 0.04 and 0.08 at room temperature and frequency of 1 MHz. 85

4.36 Dielectric constants of $Bi_{3.36+x}Mg_{1.92-y}Nb_{2.72-x+y}O_{13.76-x+(3/2)y}$ 86 pyrochlores, SS1 with x = -0.01, 0.04, 0.09, 0.14, 0.19; y = 0.06, 0.08, 0.10, 0.12 and 0.14 at frequency of 1 MHz.

4.37 Dielectric constants of $Bi_{3.36+x}Mg_{1.92-y}Nb_{2.72-x+y}O_{13.76-x+(3/2)y}$ pyrochlores, SS2 with y = 0.04; x = 0.00, 0.04 and 0.08 pyrochlores at frequency of 1 MHz. 86

4.38 Dielectric losses of $Bi_{3.36+x}Mg_{1.92-y}Nb_{2.72-x+y}O_{13.76-x+(3/2)y}$ pyrochlores, SS1 with x = -0.01, 0.04, 0.09, 0.14, 0.19; y = 0.06, 0.08, 0.10, 0.12 and 0.14 at frequency of 1 MHz. 87

4.39 Dielectric losses of $Bi_{3.36+x}Mg_{1.92-y}Nb_{2.72-x+y}O_{13.76-x+(3/2)y}$ pyrochlores, SS2 with y = 0.04; x = 0.00, 0.04 and 0.08 at frequency of 1 MHz. 87

4.40 Variation of (a) dielectric constant, (b) dielectric loss (× 10^{-3}), (c) TCε' and (d) activation energy of compositions in the BMN pyrochlore solid solution area at room temperature and frequency of 1 MHz. 88

4.41 (a) The permittivity, ε' and (b) dielectric loss, tan δ of $Bi_{3.55}Mg_{1.78}Nb_{2.67}O_{13.78}$ at different frequencies as a function of temperature in the range 10-320 K. 91

4.42 The inverse of real part of permittivity as a function of temperature as different frequencies. The inset (i) indicates the experimental data of the sample fitting to the Curie-Weiss law. 93

4.43 ln $(1/\varepsilon' - 1/\varepsilon_{max})$ against ln $(T - T_m)$ of sample 83 at different frequencies. 94

4.44 Frequencies and temperatures of ε'_{max} with fits to the Vogel-Fulcher equation as f_{max} as a function of T_{max} and the inset (i) is Arrhenius plot of log f_m as a function of $1/(T_m - T_{vf})$. 95

4.45 Capacitance, C' as a function of frequency for (a) 10-100 K, (b) 110-170 K, (c) 180-210 K, (d) 220-320 K and (e) 373-1073 K. 96

4.46 Admittance, Y' as a function of frequency for (a) 10-240 K and (b) 673-1073 K. 97

4.47 Equivalent circuits showing different R, C, CPE combinations. 98

4.48 Fit of the 10 K, 110 K, 120 K and 200 K data to circuit in Figure 4.46. 99

4.49 Temperature dependence of (a) capacitance C_1 and C_2, (b) resistance R_2 and (c) CPE_2 and the n values. 101

4.50 XRD patterns of $(Bi_{3.50}Mg_{0.50})(Mg_{1.30-x}Zn_xNb_{2.70})O_{13.80}$ ($0 \leq x \leq 0.60$) pyrochlores. 107

4.51 XRD patterns of $(Bi_{3.50}Mg_{0.50-x}Cd_x)(Mg_{1.30}Nb_{2.70})O_{13.80}$ (a) $0 \leq x \leq 0.30$; (b) $0.40 \leq x \leq 0.60$ pyrochlores. 107

4.52 XRD patterns of $(Bi_{3.50}Mg_{0.50})(Mg_{1.30-x}Ni_xNb_{2.70})O_{13.80}$ ($0.00 \leq x \leq 0.30$) pyrochlores. 108

4.53 Lattice parameters versus x in $(Bi_{3.50}Mg_{0.50})(Mg_{1.30-x}N_xNb_{2.70})O_{13.80}$ (N = Zn and Ni) and $(Bi_{3.50}Mg_{0.50-x}Cd_x)(Mg_{1.30}Nb_{2.70})O_{13.80}$ pyrochlores. 110

4.54 Williamson-Hall plots of $(Bi_{3.50}Mg_{0.50})(Mg_{1.30-x}Zn_xNb_{2.70})O_{13.80}$ ($0 \leq x \leq 0.40$) pyrochlores. 111

4.55 Williamson-Hall plots of $(Bi_{3.50}Mg_{0.50-x}Cd_x)(Mg_{1.30}Nb_{2.70})O_{13.80}$ ($0.10 \leq x \leq 0.30$) pyrochlores. 112

4.56 Scherrer equation and Williamson-Hall plots of $(Bi_{3.50}Mg_{0.50})(Mg_{1.30-x}Zn_xNb_{2.70})O_{13.80}$ ($0 \leq x \leq 0.40$) pyrochlores. 112

4.57 Scherrer equation and Williamson-Hall plots of $(Bi_{3.50}Mg_{0.50-x}Cd_x)(Mg_{1.30}Nb_{2.70})O_{13.80}$ ($0.10 \leq x \leq 0.30$) pyrochlores. 113

4.58 SEM micrographs of $(Bi_{3.50}Mg_{0.50})(Mg_{1.30-x}Zn_xNb_{2.70})O_{13.80}$ ($0 \leq x \leq 0.40$) pyrochlores. 113

4.59 SEM micrograph of $(Bi_{3.50}Mg_{0.50-x}Cd_x)(Mg_{1.30}Nb_{2.70})O_{13.80}$ ($0.10 \leq x \leq 0.30$) pyrochlores. 115

4.60 SEM micrograph of $(Bi_{3.50}Mg_{0.50})(Mg_{1.30-x}Ni_xNb_{2.70})O_{13.80}$ ($x = 0.10$) pyrochlore. 117

4.61 TGA thermograms of $(Bi_{3.50}Mg_{0.50})(Mg_{1.30-x}Zn_xNb_{2.70})O_{13.80}$ ($0 \leq x \leq 0.40$) pyrochlores. 119

4.62 TGA thermograms of $(Bi_{3.50}Mg_{0.50-x}Cd_x)(Mg_{1.30}Nb_{2.70})O_{13.80}$ ($0.00 \leq x \leq 0.30$) pyrochlores. 119

4.63 TGA thermograms of $(Bi_{3.50}Mg_{0.50})(Mg_{1.30-x}Ni_xNb_{2.70})O_{13.80}$ ($0.00 \leq x \leq 0.10$) pyrochlores. 120

4.64 DTA thermograms of $(Bi_{3.50}Mg_{0.50})(Mg_{1.30-x}Zn_xNb_{2.70})O_{13.80}$ ($0 \leq x \leq 0.40$) pyrochlores. 120

4.65 DTA thermograms of $(Bi_{3.50}Mg_{0.50-x}Cd_x)(Mg_{1.30}Nb_{2.70})O_{13.80}$ ($0.00 \leq x \leq 0.30$) pyrochlores. 121

4.66 DTA thermograms of $(Bi_{3.50}Mg_{0.50})(Mg_{1.30-x}Ni_xNb_{2.70})O_{13.80}$ (x = 0.10) pyrochlore. 121

4.67 Conductivity Arrhenius plots of $(Bi_{3.50}Mg_{0.50})(Mg_{1.30-x}Zn_xNb_{2.70})O_{13.80}$ $(0 \leq x \leq 0.40)$ pyrochlores. 122

4.68 Conductivity Arrhenius plots of $(Bi_{3.50}Mg_{0.50-x}Cd_x)(Mg_{1.30}Nb_{2.70})O_{13.80}$ $(0.00 \leq x \leq 0.30)$ pyrochlores. 123

4.69 Conductivity Arrhenius plots of $(Bi_{3.50}Mg_{0.50})(Mg_{1.30-x}Ni_xNb_{2.70})O_{13.80}$ $(0.00 \leq x \leq 0.10)$ pyrochlores. 123

4.70 Dielectric constants of $(Bi_{3.50}Mg_{0.50})(Mg_{1.30-x}Zn_xNb_{2.70})O_{13.80}$ $(0 \leq x \leq 0.40)$ pyrochlores at frequency of 1 MHz and room temperature. 125

4.71 Dielectric constants of $(Bi_{3.50}Mg_{0.50-x}Cd_x)(Mg_{1.30}Nb_{2.70})O_{13.80}$ $(0.00 \leq x \leq 0.30)$ pyrochlores at frequency of 1 MHz and room temperature. 125

4.72 Dielectric constants of $(Bi_{3.50}Mg_{0.50})(Mg_{1.30-x}Ni_xNb_{2.70})O_{13.80}$ $(0.00 \leq x \leq 0.10)$ pyrochlores at frequency of 1 MHz and room temperature. 126

4.73 Dielectric losses of $(Bi_{3.50}Mg_{0.50})(Mg_{1.30-x}Zn_xNb_{2.70})O_{13.80}$ $(0 \leq x \leq 0.40)$ pyrochlores at frequency of 1 MHz and room temperature. 126

4.74 Dielectric losses of $(Bi_{3.50}Mg_{0.50-x}Cd_x)(Mg_{1.30}Nb_{2.70})O_{13.80}$ $(0.00 \leq x \leq 0.30)$ at frequency of 1 MHz and room temperature. 127

4.75 Figure 4.74: Dielectric losses of $(Bi_{3.50}Mg_{0.50})(Mg_{1.30-x}Ni_xNb_{2.70})O_{13.80}$ $(0.00 \leq x \leq 0.10)$ at frequency of 1 MHz and room temperature. 127

4.76 Variation of dielectric constants with x in $(Bi_{3.50}Mg_{0.50})(Mg_{1.30-x}N_xNb_{2.70})O_{13.80}$ (N = Zn and Ni) and $(Bi_{3.50}Mg_{0.50-x}Cd_x)(Mg_{1.30}Nb_{2.70})O_{13.80}$ pyrochlores. 128

4.78 Variation of dielectric losses with x in $(Bi_{3.50}Mg_{0.50})(Mg_{1.30-x}N_xNb_{2.70})O_{13.80}$ (N = Zn and Ni) and $(Bi_{3.50}Mg_{0.50-x}Cd_x)(Mg_{1.30}Nb_{2.70})O_{13.80}$ pyrochlores. 128

4.79 XRD patterns of composition $Bi_3Mg_2Ta_3O_{14}$ in sintering temperature range of 900 °C - 1100 °C. 133

4.80 XRD patterns of composition $Bi_4Mg_{4/3}Ta_{8/3}O_{14}$ in sintering temperature range of 900 °C - 1025 °C. 134

4.81 Isothermal sections in Bi_2O_3-MgO-Ta_2O_5 ternary system. 136

4.82 Subsolidus phase diagram of Bi_2O_3-MgO-Ta_2O_5 ternary system. 137

4.83 Partial subsolidus phase diagram of the Bi_2O_3-MgO-Ta_2O_5. 138

4.84 Subsolidus cubic pyrochlore area in different Bi_2O_3-M-Nb_2O_5/Ta_2O_5 ternary system. 143

4.85 Expanded cubic pyrochlore solid solution area superposed on the compositional grid with x and y as variables in the formula, $Bi_{3.56-x}Mg_{1.96-y}Ta_{2.48+x+y}O_{13.50+x+(3/2)y}$. 144

4.86 Location of subsolidus compositions of $Bi_{3.56-x}Mg_{1.96-y}Ta_{2.48+x+y}O_{13.50+x+(3/2)y}$, SS3 (x = 0.01, 0.06, 0.11, 0.16, 0.21, 0.26; y = 0.18, 0.16, 0.14, 0.12, 0.10, 0.08) in the Bi_2O_3-MgO-Ta_2O_5 ternary system. 146

4.87 XRD patterns of $Bi_{3.56-x}Mg_{1.96-y}Ta_{2.48+x+y}O_{13.50+x+(3/2)y}$ pyrochlores, SS3 (a) x = 0.01, 0.11, 0.16, 0.21, 0.26; y = 0.18, 0.16, 0.14, 0.12, 0.10, 0.08; (b) x = -0.04, 0.31; y = 0.20, 0.06. 147

4.88 Location of subsolidus compositions $Bi_{3.56-x}Mg_{1.96-y}Ta_{2.48+x+y}O_{13.50+x+(3/2)y}$, SS4 (x = 0.00, 0.08, 0.16, 0.24 and 0.32; y = 0.00) in the Bi_2O_3-MgO-Ta_2O_5 ternary system. 148

4.89 XRD patterns of $Bi_{3.56-x}Mg_{1.96-y}Ta_{2.48+x+y}O_{13.50+x+(3/2)y}$ pyrochlores, SS4 (a) $0.00 \leq x \leq 0.32$; y = 0.00; (b) x = 0.34; y = 0.00. 149

4.90 Location of subsolidus compositions $Bi_{3.56-x}Mg_{1.96-y}Ta_{2.48+x+y}O_{13.50+x+(3/2)y}$, SS5 (y = 0.00, 0.08, 0.12, 0.20; x = 0.00) in the Bi_2O_3-MgO-Ta_2O_5 ternary system. 150

4.91 XRD patterns of $Bi_{3.56-x}Mg_{1.96-y}Ta_{2.48+x+y}O_{13.50+x+(3/2)y}$ pyrochlores, SS5 (a) $0.00 \leq y \leq 0.20$; x = 0.00; (b) y = 0.24; x = 0.00. 151

4.92 Variation of lattice parameters of $Bi_{3.56-x}Mg_{1.96-y}Ta_{2.48+x+y}O_{13.50+x+(3/2)y}$ pyrochlores, SS3 with x = 0.01, 0.11, 0.16, 0.21, 0.26; y = 0.18, 0.16, 0.14, 0.12, 0.10 and 0.08. 153

4.93 Variation of lattice parameters of $Bi_{3.56-x}Mg_{1.96-y}Ta_{2.48+x+y}O_{13.50+x+(3/2)y}$ pyrochlores, SS4 with y = 0.00; $0.00 \leq x \leq 0.32$. 154

4.94 Variation of lattice parameters of $Bi_{3.56-x}Mg_{1.96-y}Ta_{2.48+x+y}O_{13.50+x+(3/2)y}$ pyrochlores, SS5 with x = 0.00; $0.00 \leq y \leq 0.20$. 155

4.95 DTA thermograms of $Bi_{3.56-x}Mg_{1.96-y}Ta_{2.48+x+y}O_{13.50+x+(3/2)y}$ pyrochlores, SS3 with x = 0.01, 0.11, 0.16, 0.21, 0.26; y = 0.18, 157

0.16, 0.14, 0.12, 0.10, 0.08.

4.96 DTA thermograms of $Bi_{3.56-x}Mg_{1.96-y}Ta_{2.48+x+y}O_{13.50+x+(3/2)y}$ pyrochlores, SS4 with y = 0.00; $0.00 \leq x \leq 0.32$. 157

4.97 DTA thermograms of $Bi_{3.56-x}Mg_{1.96-y}Ta_{2.48+x+y}O_{13.50+x+(3/2)y}$ pyrochlores, SS5 with x = 0.00; $0.00 \leq y \leq 0.20$. 158

4.98 TGA thermograms of $Bi_{3.56-x}Mg_{1.96-y}Ta_{2.48+x+y}O_{13.50+x+(3/2)y}$ pyrochlores, SS3 with x = 0.01, 0.11, 0.16, 0.21, 0.26; y = 0.18, 0.16, 0.14, 0.12, 0.10, 0.08. 158

4.99 TGA thermograms of $Bi_{3.56-x}Mg_{1.96-y}Ta_{2.48+x+y}O_{13.50+x+(3/2)y}$ pyrochlores, SS4 with y = 0.00; $0.00 \leq x \leq 0.32$. 159

4.100 TGA thermograms of $Bi_{3.56-x}Mg_{1.96-y}Ta_{2.48+x+y}O_{13.50+x+(3/2)y}$ pyrochlores, SS5 with x = 0.00; $0.00 \leq y \leq 0.20$. 159

4.101 IR spectra of $Bi_{3.56-x}Mg_{1.96-y}Ta_{2.48+x+y}O_{13.50+x+(3/2)y}$ pyrochlores, SS3 with x = 0.01, 0.06, 0.11, 0.16, 0.21, 0.26; y = 0.18, 0.16, 0.14, 0.12, 0.10 and 0.08. 161

4.102 IR spectra of $Bi_{3.56-x}Mg_{1.96-y}Ta_{2.48+x+y}O_{13.50+x+(3y/2)}$ pyrochlores, SS4 with y = 0.00; x = 0.00, 0.08, 0.16, 0.24 and 0.32. 161

4.103 IR spectra $Bi_{3.56-x}Mg_{1.96-y}Ta_{2.48+x+y}O_{13.50+x+3y/2}$ pyrochlores, SS5 with x = 0.00; $0.00 \leq y \leq 0.20$. 162

4.104 Raman spectra of $Bi_{3.56-x}Mg_{1.96-y}Ta_{2.48+x+y}O_{13.50+x+(3/2)y}$ pyrochlores, SS4 with y = 0.00; x = 0.00, 0.08, 0.16, 0.24 and 0.32. 164

4.105 Raman spectra of $Bi_{3.56-x}Mg_{1.96-y}Ta_{2.48+x+y}O_{13.50+x+(3/2)y}$ pyrochlores, SS5 with x = 0.00; $0.00 \leq y \leq 0.20$. 164

4.106 Williamson-Hall plots of $Bi_{3.56-x}Mg_{1.96-y}Ta_{2.48+x+y}O_{13.50+x+(3/2)y}$ pyrochlores, SS3 with x = 0.01, 0.06, 0.11, 0.16, 0.21, 0.26; y = 0.18, 0.16, 0.14, 0.12, 0.10, 0.08. 167

4.107 Williamson-Hall plots of $Bi_{3.56-x}Mg_{1.96-y}Ta_{2.48+x+y}O_{13.50+x+(3/2)y}$ pyrochlores, SS4 with y = 0.00; $0.00 \leq x \leq 0.32$. 167

4.108 Williamson-Hall plots of $Bi_{3.56-x}Mg_{1.96-y}Ta_{2.48+x+y}O_{13.50+x+3y/2}$ pyrochlores, SS5 with x = 0.00; $0.00 \leq y \leq 0.20$. 168

4.109 Scherrer equation and Williamson-Hall plots of $Bi_{3.56-x}Mg_{1.96-y}Ta_{2.48+x+y}O_{13.50+x+(3/2)y}$ pyrochlores, SS3 with x = 0.01, 0.06, 0.11, 0.16, 0.21, 0.26; y = 0.18, 0.16, 0.14, 0.12, 0.10, 0.08. 168

4.110 Scherrer equation and Williamson-Hall plots of $Bi_{3.56-x}Mg_{1.96-y}Ta_{2.48+x+y}O_{13.50+x+(3y/2)}$ pyrochlores, SS4 with y = 0.00; 0.00 ≤ x ≤ 0.32. 169

4.111 Scherrer equation and Williamson-Hall plots of $Bi_{3.56-x}Mg_{1.96-y}Ta_{2.48+x+y}O_{13.50+x+3y/2}$ pyrochlores, SS5 with x = 0.00; 0.00≤ y ≤ 0.20. 169

4.112 The SEM micrographs of $Bi_{3.56-x}Mg_{1.96-y}Ta_{2.48+x+y}O_{13.50+x+(3/2)y}$ pyrochlores, SS3 with x = 0.01,0.06, 0.11, 0.16, 0.21, 0.26; y = 0.18, 0.16, 0.14, 0.12, 0.10, 0.08. 170

4.113 The SEM micrographs of $Bi_{3.56-x}Mg_{1.96-y}Ta_{2.48+x+y}O_{13.50+x+(3y/2)}$ pyrochlores, SS4 with y = 0.00; 0.00 ≤ x ≤ 0.32. 173

4.114 The SEM micrographs of $Bi_{3.56-x}Mg_{1.96-y}Ta_{2.48+x+y}O_{13.50+x+3y/2}$ pyrochlores, SS5 with x = 0.00; 0.00 ≤ y ≤ 0.20. 175

4.115 Arrhenius conductivity plots of $Bi_{3.56-x}Mg_{1.96-y}Ta_{2.48+x+y}O_{13.50+x+(3/2)y}$ pyrochlores, SS3 with x = 0.01, 0.06, 0.11, 0.16, 0.21, 0.26; y = 0.18, 0.16, 0.14, 0.12, 0.10, 0.08. 179

4.116 Arrhenius conductivity plots of $Bi_{3.56-x}Mg_{1.96-y}Ta_{2.48+x+y}O_{13.50+x+(3/2)}$ pyrochlores, SS4 with y = 0.00; 0.00≤ x ≤ 0.32. 179

4.117 Arrhenius conductivity plots of $Bi_{3.56}Mg_{1.96-y}Ta_{2.48+y}O_{13.50+3y/2}$ pyrochlores, SS5 with x = 0.00; 0.00 ≤ y ≤ 0.20. 180

4.118 Dielectric constants of $Bi_{3.56-x}Mg_{1.96-y}Ta_{2.48+x+y}O_{13.50+x+(3/2)y}$ pyrochlores, SS3 with x = 0.01, 0.06, 0.11, 0.16, 0.21, 0.26; y = 0.18, 0.16, 0.14, 0.12, 0.10, 0.08 as a function of temperature. 118

4.119 Dielectric constants of $Bi_{3.56-x}Mg_{1.96-y}Ta_{2.48+x+y}O_{13.50+x+3y/2}$ pyrochlores, SS4 with y =0.00; 0.00≤ x ≤ 0.32 as a function of temperature. 119

4.120 Dielectric constants of $Bi_{3.56-x}Mg_{1.96-y}Ta_{2.48+x+y}O_{13.50+x+3y/2}$ pyrochlores, SS5 with x = 0.00; 0.00≤ y ≤ 0.20 as a function of temperature. 182

4.121 Dielectric losses of pyrochlores in SS3, $Bi_{3.56-x}Mg_{1.96-y}Ta_{2.48+x+y}O_{13.50+x+(3/2)y}$ (x = 0.01, 0.06, 0.11, 0.16, 0.21, 0.26; y = 0.18, 0.16, 0.14, 0.12, 0.10, 0.08) as a function of temperature. 183

4.122 Dielectric losses of $Bi_{3.56-x}Mg_{1.96-y}Ta_{2.48+x+y}O_{13.50+x+(3y/2)}$ (0.00 ≤ x ≤ 0.32; y = 0.00) pyrochlores as a function of temperature. 184

4.123 Dielectric losses of $Bi_{3.56-x}Mg_{1.96-y}Ta_{2.48+x+y}O_{13.50+x+3y/2}$ (0.00 ≤ y ≤ 184

0.20; x = 0.00) pyrochlores as a function of temperature.

4.124 Variation of (a) dielectric constant, (b) dielectric loss (× 10^{-3}), (c) TCε' and (d) activation energy of compositions in the BMT pyrochlore solid solution area at room temperature and frequency of 1 MHz. 186

4.125 Cole-cole plots of $Bi_{3.55}Mg_{1.78}Ta_{2.67}O_{13.78}$ at (a) 550 - 700 °C and (b) 749 - 851 °C; (i) parallel RC circuit. 189

4.126 Combined spectroscopic plots of $Bi_{3.55}Mg_{1.78}Ta_{2.67}O_{13.78}$ at 598 °C. 190

4.127 Imaginary part of impedance of $Bi_{3.55}Mg_{1.78}Ta_{2.67}O_{13.78}$ as a function of frequency at different temperatures. 190

4.128 Arrhenius plot for the peak frequency and the conductivity Arrhenius plot of $Bi_{3.55}Mg_{1.78}Ta_{2.67}O_{13.78}$. 191

4.129 The permittivity, ε' and (b) dielectric loss, tan δ of $Bi_{3.30}Mg_{1.88}Ta_{2.82}O_{13.88}$ at different frequencies as a function of temperature in the range 20-320 K. 193

4.130 The inverse of real part of permittivity as a function of temperature as different frequencies. The inset (i) indicates the experimental data of the sample fitting to the Curie-Weiss law. 195

4.131 ln ($1/\varepsilon' - 1/\varepsilon_{max}$) against ln ($T - T_m$) of sample 75 at different frequencies. 196

4.132 Frequencies and temperatures of ε'_{max} with fits to the Vogel-Fulcher equation as (a) f_{max} as a function of T_{max} and (b) Arrhenius plot of log f_m as a function of $1/(T_m - T_{vf})$. 197

4.133 Capacitance, C' as a function of frequency for (a) 20 - 70 K, (b) 80 - 130 K, (c) 140 - 170 K, (d) 180 - 320 K and (e) 373 - 1073 K. 198

4.134 Admittance, Y' as a function of frequency for (a) 20 - 160 K and (b) 673 - 1123 K. 199

4.135 Equivalent circuits showing different R, C, CPE combinations. 201

4.136 Fit of the 20 K, 100 K, 120 K and 150 K data to circuit in Figure 4.131. 201

4.137 Temperature dependence of (a) capacitance C_1 and C_2, (b) resistance R_2 and (c) CPE_2 and the n values. 204

4.138 XRD patterns of (a) $(Bi_{3.50}Mg_{0.50})(Mg_{1.30-x}Zn_xTa_{2.70})O_{13.80}$ ($0 \leq x \leq 1.00$) solid solution; (b) $x = 0.80$. 210

4.139 XRD patterns of $(Bi_{3.50}Mg_{0.50-x}Cd_x)(Mg_{1.30}Ta_{2.70})O_{13.80}$ ($0 \leq x \leq 0.30$) solid solution. 211

4.140 XRD patterns of $(Bi_{3.50}Mg_{0.50})(Mg_{1.30-x}Ni_xTa_{2.70})O_{13.80}$ ($0 \leq x \leq 0.30$) solid solution. 212

4.141 Lattice parameters of $(Bi_{3.50}Mg_{0.50})(Mg_{1.30-x}M_xTa_{2.70}O_{13.80}$ (M = Zn and Ni) and $(Bi_{3.50}Mg_{0.50-x}Cd_x)(Mg_{1.30}Ta_{2.70}O_{13.80}$ pyrochlores. 213

4.142 SEM micrographs of of $(Bi_{3.50}Mg_{0.50})(Mg_{1.30-x}Zn_xTa_{2.70})O_{13.80}$ ($0 \leq x \leq 0.60$). 214

4.143 SEM micrographs of of $(Bi_{3.50}Mg_{0.50-x}Cd_x)(Mg_{1.30}Ta_{2.70})O_{13.80}$, $x = 0.10$. 216

4.144 SEM micrographs of of $(Bi_{3.50}Mg_{0.50})(Mg_{1.30-x}Ni_xTa_{2.70})O_{13.80}$, $x = 0.10$. 216

4.145 Scherrer equation and Williamson-Hall plots of $(Bi_{3.50}Mg_{0.50})(Mg_{1.30-x}Zn_xTa_{2.70})O_{13.80}$, $0.00 \leq x \leq 0.60$. 217

4.146 TGA thermograms of of $(Bi_{3.50}Mg_{0.50})(Mg_{1.30-x}Zn_xTa_{2.70})O_{13.80}$ ($0 \leq x \leq 0.60$). 219

4.147 TGA thermograms of of $(Bi_{3.50}Mg_{0.50})(Mg_{1.30-x}Ni_xTa_{2.70}O_{13.80}$ and $(Bi_{3.50}Mg_{0.50-x}Cd_x)(Mg_{1.30}Ta_{2.70}O_{13.80}$ pyrochlores. 219

4.148 DTA thermograms of of $(Bi_{3.50}Mg_{0.50})(Mg_{1.30-x}Zn_xTa_{2.70})O_{13.80}$ ($x = 0.20 - 0.60$) pyrochlores. 220

4.149 DTA thermograms of of $(Bi_{3.50}Mg_{0.50})(Mg_{1.30-x}Ni_xTa_{2.70}O_{13.80}$ and $(Bi_{3.50}Mg_{0.50-x}Cd_x)(Mg_{1.30}Ta_{2.70}O_{13.80}$ pyrochlores. 220

4.150 Arrhenius conductivity plots of $(Bi_{3.50}Mg_{0.50})(Mg_{1.30-x}Zn_xTa_{2.70})O_{13.80}$ ($0 \leq x \leq 0.60$). 223

4.151 Arrhenius conductivity plots of $(Bi_{3.50}Mg_{0.50-x}Cd_x)(Mg_{1.30}Ta_{2.70}O_{13.80}$ ($0 \leq x \leq 0.10$) pyrochlores. 223

4.152 Arrhenius conductivity plots of $(Bi_{3.50}Mg_{0.50})(Mg_{1.30-x}Ni_xTa_{2.70})O_{13.80}$ ($0 \leq x \leq 0.10$). 224

4.153 Dielectric constants of $(Bi_{3.50}Mg_{0.50})(Mg_{1.30-x}M_xTa_{2.70}O_{13.80}$ (M = Zn and Ni) and $(Bi_{3.50}Mg_{0.50-x}Cd_x)(Mg_{1.30}Ta_{2.70}O_{13.80}$ pyrochlores. 224

4.154 Dielectric losses of $(Bi_{3.50}Mg_{0.50})(Mg_{1.30-x}M_xTa_{2.70}O_{13.80}$ (M = Zn 225 and Ni) and $(Bi_{3.50}Mg_{0.50-x}Cd_x)(Mg_{1.30}Ta_{2.70}O_{13.80}$ pyrochlores.

4.155 XRD patterns of $(Bi_{3.50}Mg_{0.50})(Mg_{1.30}Nb_xTa_{2.70-x})O_{13.80}$ $(0.00 \leq x \leq 2.70)$. 226

4.156 Lattice parameters of $(Bi_{3.50}Mg_{0.50})(Mg_{1.30}Nb_xTa_{2.70-x})O_{13.80}$ $(0.00 \leq x \leq 2.70)$. 226

4.157 SEM micrographs of $(Bi_{3.50}Mg_{0.50})(Mg_{1.30}Nb_xTa_{2.70-x})O_{13.80}$ $(0.00 \leq x \leq 2.70)$. 228

4.158 Williamson-Hall plots of $(Bi_{3.50}Mg_{0.50})(Mg_{1.30}Nb_xTa_{2.70-x})O_{13.80}$ $(0.00 \leq x \leq 2.70)$. 229

4.159 Williamson-Hall and Scherrer plots of $(Bi_{3.50}Mg_{0.50})(Mg_{1.30}Nb_xTa_{2.70-x})O_{13.80}$ $(0.00 \leq x \leq 2.70)$. 229

4.160 DTA thermograms of of $(Bi_{3.50}Mg_{0.50})(Mg_{1.30}Nb_xTa_{2.70-x})O_{13.80}$ pyrochlores. 230

4.161 TGA thermograms of of $(Bi_{3.50}Mg_{0.50})(Mg_{1.30}Nb_xTa_{2.70-x})O_{13.80}$ pyrochlores. 231

4.162 Arrhenius conductivity plots of $(Bi_{3.50}Mg_{0.50})(Mg_{1.30}Nb_xTa_{2.70-x})O_{13.80}$ $(0.00 \leq x \leq 2.70)$. 233

4.163 Dielectric constants as a function of temperatures of $(Bi_{3.50}Mg_{0.50})(Mg_{1.30}Nb_xTa_{2.70-x})O_{13.80}$ $(0.00 \leq x \leq 2.70)$. 233

4.164 Dielectric losses as a function of temperatures of $(Bi_{3.50}Mg_{0.50})(Mg_{1.30}Nb_xTa_{2.70-x})O_{13.80}$ $(0.00 \leq x \leq 2.70)$. 235

4.165 Dielectric constant and dielectric losses with variation of x in $(Bi_{3.50}Mg_{0.50})(Mg_{1.30}Nb_xTa_{2.70-x})O_{13.80}$ $(0.00 \leq x \leq 2.70)$. 235

LIST OF ABBREVATIONS

3-D	three dimensions
ac	alternating current
ATR	attenuated total reflectance
BVS	bond valence sum
dc	direct current
CPE	constant phase element
DPT	diffuse phase transition
DTA	differential thermal analysis
EIA	electronic industries alliance
FT-IR	fourier-transform infrared spectroscopy
FWHM	full width at half maximum
ICDD	international centre for diffraction data
ICP-OES	inductively coupled plasma-optical emission spectrometry
IEEE	institute of electrical and electronics engineers
IS	impedance spectroscopy
JCPDS	Joint Committee on Powder Diffraction Standard
LTCC	low temperature cofired ceramics
MLCC	multilayer ceramic capacitor
NPO	negative, positive, but almost zero temperature coefficient of capacitance
PCB	printed circuit board
PLD	pulsed laser deposition
ppm	parts per million
SEM	scanning electron microscopy

TCC	temperature coefficient of capacitance
TCε	temperature coefficient of permittivity
TCF	temperature coefficient of resonance frequency
TGA	thermogravimetry analysis
W-H	Williamson and Hall
XRD	X-ray Diffraction
a, b, c, α, β, γ	lattice parameters
A	area
C	capacitance
C_b	bulk capacitance
C_o	vacuum capacitance
C_{gb}	grain boundary capacitance
d	d-spacing
D	diameter
Ea	activation energy
eV	electron volt
f	frequency
f_r	resonance frequency
h, k, l	miller indices
I	current
k	Boltzmann’s constant
K	Kelvin
l	thickness
M*	complex electric modulus
M’	real part of electric modulus

M''	imaginary part of electric modulus
Q_f	quality factor
R	resistance
R_b	bulk resistance
R_{dc}	dc resistance
R_{gb}	grain boundary resistance
R_{sl}	resistive surface layer
RC	resistor-capacitor
T	temperature
T_B	Burns temperature
T_c	Curie temperature
T_m	maxima temperature
T_o	Curie-Weiss temperature
T_{vf}	freezing temperature
V	voltage
ω	angular frequency
Y^*	complex admittance
Y'	real part of admittance
Y''	imaginary part of admittance
Z	impedance
Z^*	complex impedance
Z'	real part of impedance
Z''	imaginary part of impedance
α_1	linear thermal expansion coefficient
Ω	ohm

ρ	resistivity
ε^*	complex permittivity
ε'	real part of permittivity
ε''	imaginary part of permittivity
ε_{max}	maxima of permittivity
ε_o	absolute permittivity of vacuum or in free space
ξ	electrostrictive coefficient
$\tan \delta$	dielectric loss
$\tan \delta_{max}$	maxima of dielectric loss
ω	angular frequency
χ'	dielectric susceptibility
χ_m	molar susceptibility
χ_g	gram susceptibility
λ	wavelength
λ_o	wavelength in the vacuum
σ	conductivity
σ_o	pre exponential factor
τ	relaxation time
θ	Bragg angle
γ	diffuseness constant

CHAPTER 1

INTRODUCTION

1.1 Electroceramics

Ceramic is a polycrystalline nonmetallic body, which made from powder that formed into a shape and then heating the shape to impart mechanical strength. However, this does not include single crystals, glasses and cements. Electroceramics are materials that are applicable for electrical use. They are high technological materials whose properties and applications depend on a complex interplay of structural, processing and compositional varieties. In the first half twentieth century, the characteristics of electroceramics are well known for chemically stable and high resistivity. The properties is highly diverse, e.g. mineral magnetite in ceramic form, which is recognised as having a high electrical conductivity besides to its magnetic properties (Moulson and Herbert, 1990(a); Irvine *et al*., 1990).

Advanced ceramics are an essential part of the electronic and electrical equipment that used for consumer, industrial, and military applications. The electronic ceramics are integral components of the circuits that used in computers, signal processing, telecommunications, power transmission, and power control technologies. These materials play a ubiquitous but often little-noticed role in our daily lives. The applications of electroceramics included ceramic conductors, piezoelectric ceramics, pyroelectric materials, dielectrics and insulator, low temperature cofired ceramics etc. The electroceramic that are closely related to the dielectric ceramics whose properties and applications are discussed in the subsequent section 1.2 and 1.3, respectively.

1.2 The Properties of Dielectric Materials

Dielectric materials exhibit high electrical resistivities and they are poor electrical conductor. They cover a wide range of properties, from steatite (relative permittivity, ε’ of 6) to complex ferroelectric compositions (relative permittivities, ε’ exceeding 20000). Class I dielectrics include low- and medium-permittivity ceramics and their dissipation factors are less than 0.003. The medium-permittivity covers ε’ in the range of 15 - 500 with temperature coefficients of permittivity in the range of 100 to -2000 MK^{-1}. Class II dielectrics consist of high-permittivity ceramics based on ferroelectrics whose ε’ values are between 2000 - 20000 within varying temperature, field strength and frequency. The dissipation factors of these materials are normally below 0.03, but could be at higher level in certain temperature ranges especially when high AC fields are applied. Class III dielectrics contain a conductive phase that effectively reduces the thickness of dielectric in capacitors by at least an order of magnitude (Moulson and Herbert, 1990(c); Herbert, 1985).

1.2.1 Polarisability

When an electric field is applied to an ideal dielectric material, there is no long-range transport of charge but only limited rearrangement such that the dielectric acquires a dipole moment. This situation is said to be polarised. There are basically four types of polarisation mechanisms in dielectric materials and the details for each mechanism is described in the next section (Moulson and Herbert, 1990(b)). The polarisation gives rise to useful behaviour, such as electrical energy storage (capacitors) and piezoelectric effect.

1.2.1.1 Types of Polarisation Mechanism

i) Electron polarisation

This mechanism involves deformation of external electron clouds of individual atoms under the electric field. Relaxation time of this polarisation is in the range of 10^{-14} - 10^{-15} s (Nowotny and Rekas, 1992).

Figure 1.1: Electronic polarisation (Nowotny and Rekas, 1992).

ii) Space charge polarisation

It is also the Maxwell-Wagner polarisation which involves the deformation of the space charge localised at the grain boundaries and dislocations (Nowotny and Rekas, 1992). This polarisation generally found in ferrites and semiconductors when temperature increases (Gao and Sammes, 1999).

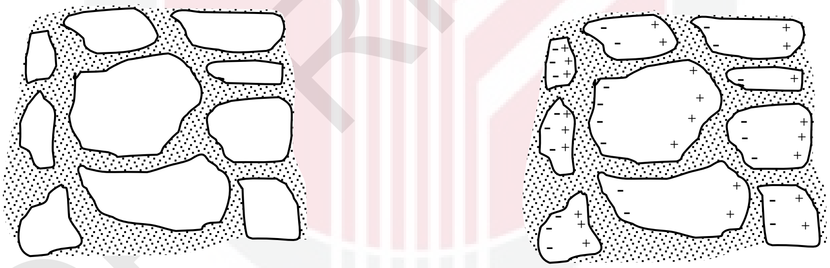

Figure 1.2: Space charge polarisation (Nowotny and Rekas, 1992).

iii) Dipole polarisation

This polarisation involves the orientation of the permanent dipoles, if present in the lattice without an electric field. Application of the field results in the change of dipoles in their orientations. The orientation time of this polarisation is much longer which they remains within 10^{-8} - 10^{-10} s (Nowotny and Rekas, 1992).

Figure 1.3: Dipole polarisation (Nowotny and Rekas, 1992).

iv) Ionic (atomic) polarisation

The polarisation involves a shift of lattice atoms (ions) from their equilibrium positions to more stable positions under an electric field. The charge is then slightly redistributed within the material giving rise to a relaxation time about 10^{-13} s (Gao and Sammes, 1999; Nowotny and Rekas, 1992).

+ - + - + -   +-   +-   +-

- + - + - +   -   +-   +-   +

+ - + - + -   -   +-   +-

- + - + - +   -   +-   +-   +

+ - + - + -   +-   +-   +-

Figure 1.4: Ionic (atomic) polarisation (Nowotny and Rekas, 1992).

1.2.2 Permittivity

The absolute permittivity, ε_o is the measure of the resistance of a substance when it is encountered formation of electric field. Relative permittivity or dielectric constant, ε' shows the relative permittivity value of a medium to the absolute permittivity of vacuum or in free space, ε_o where ε_o is 8.854×10^{-12} Fm^{-1}. The relative permittivity, ε' of a material shows its energy storing capacity when a potential is applied across it. It is related to the macroscopic properties like polarisation or capacitance. The permittivity of a material determines the relative speed that an electrical signal can travel in that material. A low permittivity will result in a high signal propagation speed (Sebastian, 2008(a)).

Figure 1.5 (a) illustrates a dielectric material in a situation of simply absent air (air/ vacuum). The two plates are segregated by a distance of *l* while the area of each plate is given as *A* and the plates are connected to a voltage supply, *V*. When the voltage is applied, it causes one of the plates positively charged and the other plate is negatively charged. The magnitude of charge on each plate is given by Q while the magnitude of charge per unit area is given by Q/*A*. The capacitance, C_o indicates the case of air (between the two plates) and has the unit of Coulomb/Volt (the same as Farad, F). Hence, it is given the formula as below:

$$C_o = \varepsilon_o A/l \tag{1.1}$$

where capacitance is proportional to *A* and is inversely proportional to *l* (Chung, 2010).

Figure 1.5 (b) shows a parallel-plate capacitor like which the dielectric material replaces the air with relative dielectric constant, ε'. The magnitude of charge on each plate is ε'Q instead of Q, hence the capacitance, C is given the formula as

$$C = \varepsilon' Q/V = \varepsilon' C_o = \varepsilon_o \varepsilon' A/l \tag{1.2}$$

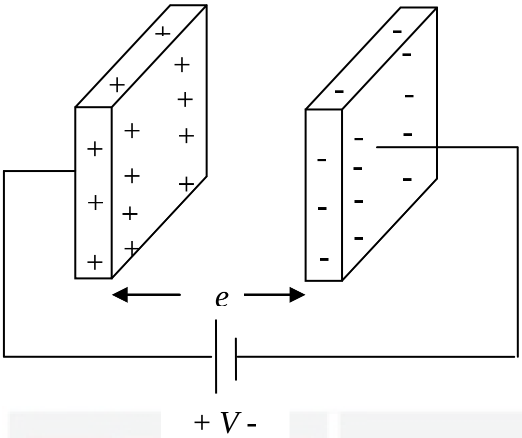

Figure 1.5 (a): A parallel-plate dielectric capacitor in the form of air separated by plates that are connected to a voltage supply, which makes one plate positively charged while the other plate is negatively charged (Chung, 2010).

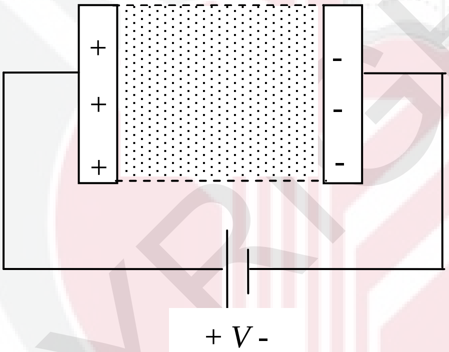

Figure 1.5 (b): A parallel-plate capacitor like that in Figure 1.5 (a), except that the air between the two plates is replaced by a dielectric material (i.e. an electrical insulator) (Chung, 2010).

1.2.3 Dielectric Loss, tan δ

Dielectric loss or dissipation factor, tan δ is the conversion of electrical energy to heat in a capacitor. This is due to the conversion of the movement of charges into vibrations of the lattice, i.e. phonons. It is expressed by the power factor, sin δ, where $(^{1}/_{2}\,\pi - \delta)$ is the advance in phase of the current relative to that of an applied alternating voltage. The power factor is the fraction of the voltage-ampere product applied to a capacitor that is lost as heat, it is usually given as a percentage and this usage is commonly extended to the dissipation factor (Moulson and Herbert, 1990(c)). The origin of dielectric losses can also be considered as a delay between the electric field and the electric displacement vectors. The total dielectric loss is the sum of intrinsic and extrinsic losses. Intrinsic dielectric losses are the losses in the perfect crystals which depend on the crystal structure. This can be described by the interaction of the phonon system with the ac electric field. Extrinsic losses are associated with imperfections in the crystal lattice which caused by impurities, microstructural defects, grain boundaries, porosity, microcracks, order-disorder, random crystallite orientation, dislocations, vacancies, dopant atoms etc (Sebastian, 2008(a)).

The dielectric loss can be portrayed using the formula as follow:

$$\tan \delta = \varepsilon''/\varepsilon' \qquad (1.3)$$

where ε' is the relative permittivity; ε'' is the imaginary part of the permittivity which termed the loss factor.

The tan δ is generally taken as an indication of the quality of a particular type of capacitor. A high loss is not preferable in almost all applications. It lowers the quality and results in the generation of heat that raises the temperature of a capacitor.

1.2.4 Temperature Coefficient of Capacitance (TCC)

Temperature coefficient of capacitance (TCC) is the maximum change in capacitance over a specific temperature range. The capacitance value stated by the manufacturer is established at a reference temperature of 25 °C to 300 °C and TCC should always be considered for applications operating above or below this temperature. It is always performed in parts per million (ppm) per degrees centigrade. The TCC is calculated as follow:

$$TCC = (C_f – C_i / (T_f - T_i)C_i) *1000000 \qquad (1.4)$$

where C_f and C_i refer to capacitance value at initial temperature, T_i and final temperature, T_f, respectively (Fiore, 2000).

1.3 Application of Dielectric Materials

Ceramic dielectrics have been produced in a wide range of compositions and forms as to fulfil the needs especially in electronic industries. Several applications of dielectric materials are presented in the coming subsections.

1.3.1 Low Temperature Cofired Ceramic (LTCC)

The LTCC has become crucial in the development of various modules and substrates. This technology combined several thin layers of low-permittivity ceramic composites and conductors. These resulted in multilayered LTCC modules that are applied in the form of a 3D wiring circuit board today. The LTCC allows a versatile mix of passive microwave components such as microstrips, striplines, antennas, filters, resonators, capacitors etc, making possible a whole matrix of design integrated components that are interconnected with 3D stripline circuitry. Among the various components that can be realised in LTCC packages are resonators and internal capacitors (Sebastian, 2008(b)).

The great advantage of LTCC technology is related to the low sintering temperature (< 950 °C), as this gives the advantageous utilisation for today's packaging concepts in microelectronic and microwave modules. This feature allows the embedded microwave components and transmission lines can be fabricated using highly conductive and inexpensive electrodes including silver, gold or copper with low conductor loss and low electrical resistance at high frequencies (Sebastian, 2008(b)).

1.3.2 High Frequency Ceramic Dielectrics

Highly frequency dielectric ceramics make it possible to markedly miniaturise passive microwave components such as resonators. The resonators are meant for the stabilisation of oscillators and frequency filters. These ceramics have to fulfil the requirements of high permittivity, extremely low dielectric losses and low temperature coefficient of the permittivity, TCε in order to yield temperature stable resonators (Wersing, 1991).

Two main types of resonators are found and these materials must have the ε' values in the range of 10 - 90 over the frequency range of 500 MHz to 30 GHz. These are coaxial λ/4 resonators filled with dielectric for frequencies up to 3 GHz. Their lengths are determined by

$$l = (\lambda_o/4)\bullet(1/\sqrt{\varepsilon'}) \qquad (1.5)$$

Resonators used in higher frequencies are made from a piece of dielectric wire. They are called dielectric resonators. Their diameters can be expressed as

$$D \approx \lambda_o\bullet\,(1/\sqrt{\varepsilon'}) \qquad (1.6)$$

with λ_o being the vacuum wavelength at the resonance frequency (Wersing, 1991).
The temperature coefficient of the resonance frequency, TCF has to be approximately zero in order to obtain temperature constant oscillators and frequency filters.

$$TCF = (1/f_r)\bullet(\partial f_r/\partial T) \approx (1/f_r\,\bullet\Delta f_r)/\Delta T \qquad (1.7)$$

Since the resonance frequency of a resonator depends on its size and on ε', the equation are given as follow:

$$TCF = -TC\varepsilon'/(2-\alpha_1) \qquad (1.8)$$

with TCε' is being defined according to TCF in (equation 1.7) and $\alpha_1$being the linear thermal expansion coefficient, i.e. the temperature coefficient of one of the resonator's dimensions e.g. the length, *l* (Wersing, 1991).

The first microwave ceramic, which fulfils the technical requirements, is $BaTi_4O_9$. Its ε' is 38 with TCF ≈ 15 ppm/K and the quality factor, $Q_f \approx 5000$ at 2 GHz. Later, $Ba_2Ti_9O_{20}$ is found to have better properties with ε' of 40, TCF ≈ 2 and $Q_f \approx 15000$ at 2 GHz. Nd_2O_3-TiO_2-BaO-Bi_2O_3 is another ceramic that is applicable as microwave ceramics with high permittivity. On the other hand, ceramic with low losses is found in the $Ba(ZnTa)O_3$ system where $Ba(Zn_{1/3}Ta_{2/3})O_3$ yielded ε' of 30, TCF ≈ 0 ppm/K and $Q_f \approx 6000$ at 11 GHz. Table 1.1 shows a collection of microwave ceramics which have gained important technical interests to date (Wersing, 1991).

Table 1.1: Today's most important group of microwave ceramics (Wersing, 1991).

Ceramic	ε'	TCF (ppm/K)	Q_f	
			2 GHz	20 GHz
$Ba_2Ti_9O_{20}$	40	2	15000	2000
$Zr_{0.8}TiSn_{0.2}O_4$	38	0	15000	3000
$BaTi_u[(Ni_xZn_{1-x})_{1/3}Ta_{2/3}]_{1-u}O_3$	30	-3…3	26000	5000

$Ba[Sn_x(Mg_{1/3}Ta_{2/3})_{1-x}]O_3$	25	≈ 0	> 40000	10000
Nd_2O_3-BaO-TiO_2-Bi_2O_3	≈90	≈0	3000	-

1.3.3 Capacitor

Ceramic capacitors have become the dominant capacitor type because they are small, reliable and they can be manufactured cost effectively through highly mechanised processes. Capacitors are valuable for the electrical energy storage. The storage of electrical energy is based on the separation between positive and negative charges. The consequences of Coulombic attraction, the separation of opposite charges costs energy. The magnitude of charge involves in the separation is greater, the more electrical energy amount can be stored (Chung, 2010; Khan *et al*., 1987). Figure 1.6 shows the assembled capacitor and disc capacitor, respectively (Khan *et al*., 1987).

Assembled capacitor

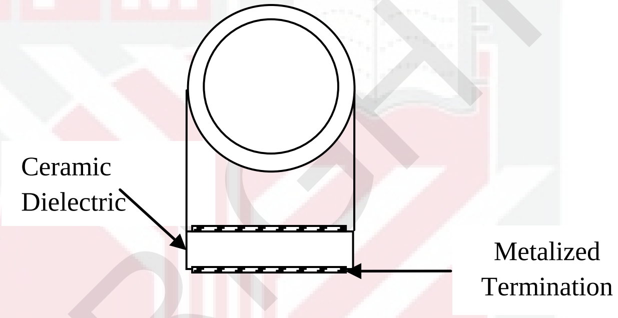

Disc capacitor

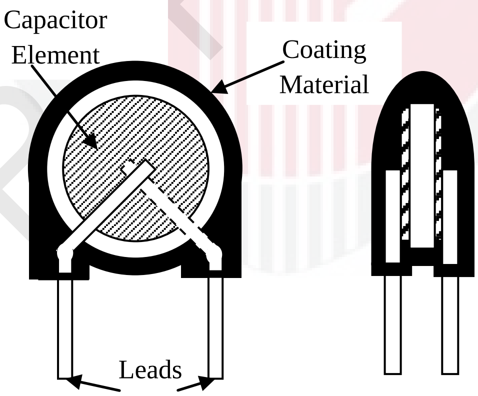

Figure 1.6: Assembled capacitor and disc capacitor, respectively (Khan *et al*., 1987).

1.3.4 Multilayer Ceramic Capacitors (MLCCs)

Multilayer ceramic capacitors (MLCCs) have grown from mica mineral capacitors that used for highly stable, good quality and small volume components in electronic systems, especially military communications equipment in 1940s (Ward, 1991). MLCCs have been in continuous development and used for over 30 years and yet still in active research development in order to enhance their quality. The use of MLCCs prevails nowadays due to their excellent properties, e.g. high capacitance, small size, high reliability and high-frequency characteristics (Kishi *et al*., 2003; Ward, 1991).

The monolithic structure of a multilayer ceramic capacitor requires that both the buried electrodes; that is the internal electrodes and the external terminations (external electrode) as well as the ceramic dielectric should be compatible with one another and during the manufacturing process. Figure 1.7 shows the cut-away view of multilayer ceramic capacitor.

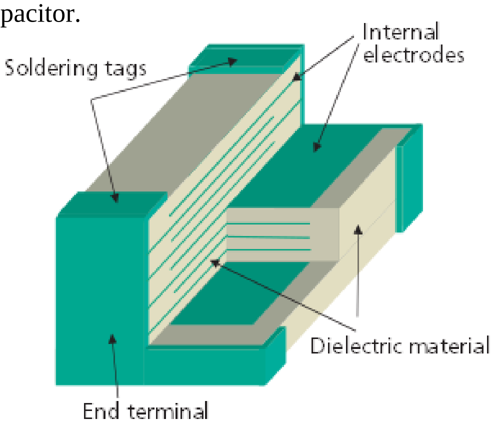

Figure 1.7: Cut-away view of multilayer ceramic capacitor (Kishi *et al*., 2003).

The first MLCC has made from polycrystalline $BaTiO_3$ ceramic since early 1950s. Conventional MLCCs based on $BaTiO_3$ are fabricated with noble metals such as platinum (Pt) or palladium (Pd) as internal electrodes which can be fired with dielectric in air at 1300 °C or even higher. With increasing stacked layers due to miniaturisation process and higher capacitance of MLCCs, the electrode cost increases steeply. Hence, silver (Ag)-Pd alloy electrodes are used to achieve low-temperature sintering of dielectrics while base metals such as nickel (Ni) and copper (Cu) are used as internal electrodes using nonreducible dielectric that can be fired in a reducing atmosphere as to cut down the internal electrode cost. On the other hand, different types of dopants introduced into $BaTiO_3$ are meant for varying the ε’ value. It can be categorised into four primary categories of dielectrics, i.e. a) high-Q_f, low-ε’ temperature compensating materials; b) intermediate-ε’ materials; labelled X7R or BX; c) high ε’ formulations, known as Z5U or Z5V and d) nonhomogeneous, barrier layer materials that have ε’ up to 100,000. Table 1.2 shows typical ceramic dielectric materials for MLCCs together with several Electronic Industries Alliance (EIA) specifications. Other dielectrics that can be sintered at low temperatures, i.e. below 1100°C, are Pb-based complex perovskite materials. Examples of Pb-based materials that are applicable as MLCCs include $Pb(Mg_{1/2}W_{1/2})O_3$, $Pb(Mg_{1/3}Nb_{2/3})O_3$, $Pb(Zn_{1/3}W_{3/3})O_3$ and $Pb(Fe_{1/3}W_{2/3})O_3$- $Pb(Fe_{1/2}Nb_{1/3})O_3$, respectively.

Table 1.2: Typical ceramic dielectric materials for MLCCs with several EIA specifications (Kishi *et al*., 2003; Khan *et al*., 1987).

EIA designation	Class	Temperature range (°C)	Temp.-cap. Change (%)	ε' value up to	$BaTiO_3$ content (%)	Other dopants	Grain size (µm)
NPO (C0G)	1	-55 to 125	±30 ppm	100	10-50	TiO_2, $CaTiO_3$, $Nd_2Ti_2O_7$	1
X7R (BX)	2	-55 to 125	±15	4,000	90-98	MgO, MnO, Nb_2O_5, CoO Rare-earth	<1.5
Z5U	2	10 to 85	+22, -56	14,000	80-90	$CaZrO_3$, $BaZrO_3$	3-10
Y5V	2	-30 to 85	+22,-82	18,000	80-90	$CaZrO_3$, $BaZrO_3$	3-10

1.3.5 Piezoelectric Ceramics

Dielectric materials that can develop electric polarisation when they are strained through an applied stress are known as piezoelectric, which means “pressure electricity”. They show the development of a strain, x which is directly proportional to an applied field. The resultant strain is proportional to the square of the field known as the electrostrictive effect. The phenomenon of electrostriction is expressed by a relationship

$$x = \xi E^2 \qquad (1.8)$$

where ξ is the electrostrictive coefficient and E is the electric field.

The most commonly used piezoelectric materials include quartz, barium titanate ($BaTiO_3$), lead titanate, lead zirconate, CdS and ZnO. The applications of these piezoelectric materials are such as gas igniters, actuators, piezoelectric transformer etc (Gao and Sammes, 1999; Moulson and Herbert, 1990(d)).

1.3.6 Pyroelectric Ceramics

Pyroelectric materials have crystal structure contains at least one crystallographic direction along which spontaneous polarisation exists. They are a special class of piezoelectrics. Heating of pyroelectric material leads to mechanical deformation because of the thermal expansion. It produces a change in extent of polarisation which then resulting in a voltage across the sample. The pyroeletricity of a material is measured by the pyroelectric temperature coefficient dP/dT as follow:

$$\Delta q/A = \Delta T dP/dT \qquad (1.9)$$

where Δ q/A is the charge released on area A when temperature changes by Δ T.

The examples of pyroelectric materials include $BaTiO_3$, $LiTaO_3$, $Pb(Zr,Ti)O_3$ etc. Pyroelectric materials are applicable as control of oscillator frequencies in the telecommunication equipment, sonar, high voltage step-up transformers, band-pass filters, and accelerometers (Gao and Sammes, 1999).

1.4 Problem statements

Bismuth zinc niobate pyrochlores (BZN) and bismuth zinc tantalate pyrochlores (BZT) are well known as dielectric materials that are applicable as multilayer ceramic capacitors. This sheds new light on the preparation of new pyrochlore through chemical doping especially MgO could offer low dielectric loss. To date, limited information is available in literature concerning the properties of pyrochlores in the Bi_2O_3-MgO-N_2O_5 (N= Nb and Ta) systems. These reported compositions may have been a mixture that contains trace amount of other secondary phases. Therefore, it is important to study the formation mechanism and to establish a suitable synthesis condition for the sample preparation. The detailed knowledge of the structure-property relations for the individual phases is still scarce, but it is especially important if these phases have variable composition and is essential in order to control and optimise the properties.

1.5 Objectives

The objectives of this research are:

I. To synthesise single phase cubic pyrochlores and their solid solutions in the Bi_2O_3-MgO-Nb_2O_5 (BMN) and Bi_2O_3-MgO-Ta_2O_5 (BMT) ternary systems.

II. To construct phase diagrams in the above mentioned systems through careful study of phase formation, phase stability, phase compatibility of BMN and BMT phases in condition of thermal equilibrium.

III. To characterise the single phase materials using X-ray diffraction analysis (XRD), Fourier transform infrared spectroscopy (FT-IR), Raman spectroscopy, thermal analysis (DTA and TGA), scanning electron microscopy (SEM), inductively coupled plasma atomic emission spectroscopy (ICP-OES) and AC impedance spectroscopy.

IV. To investigate the chemical doping effect, i.e. ZnO, NiO, CdO and Nb_2O_5 in BMN and BMT pyrochlores as to explore the possibility of new solid solution formation as well as to enhance the electrical performance.

REFERENCES

Adamczyk, M., Ujma, Z., Szymczak, L., Soszyński, A. and Koperski, J. 2007. Dielectric properties and relaxation of Bi-doped $(Pb_{0.75}Ba_{0.25})(Zr_{0.70}Ti_{0.30})O_3$ ceramics. *Materials Science and Engineering B* 136: 170-176.

Ananta, S. 2004. Effects of starting precursor and calcinations condition on phase formation characteristics of $Mg_4Nb_2O_9$ powders. *Materials Letters* 58: 2834-2841.

Ang, C., Yu, Z., Youn, H.J., Randall, C.A., Bhalla, A.S., Cross, L.E., Nino, J. and Lanagan, M. 2002. Low-temperature dielectric relaxation in the pyrochlore $(Bi_{3/4}Zn_{1/4})_2(Zn_{1/4}Ta_{3/4})_2O_7$ compound. *Applied Physics Letters* 80: 4807-4809.

Arenas, D.J., Gasparov, L.V., Qiu, W., Nino, J.C., Patterson, C.H. and Tanner, D.B. 2010. Raman study phonon modes in bismuth pyrochlores. *Physical Review B* 82: 214302.

Baskin, Y. and Schell, D.C. 1963. Phase studies in the binary system $MgO-Ta_2O_5$. *Journal of the American Ceramic Society* 46: 174-177.

Bell, A.J. 1993. Calculations of dielectric properties from the superparaelectric model of relaxors. *Journal of Physics: Condensed Matter* 5: 8773-8792.

Bing, Y.H., Bokov, A.A. and Ye, Z.G. 2011. Diffuse and sharp ferroelectric phase transitions in relaxors. *Current Applied Physics* 11: 514-521.

Bouchard, R.J. and Gillson, J.L. 1971. A new family of bismuth-precious metal pyrochlores. *Materials Research Bulletin* 6: 669-680.

Cann, D.P., Randall, C.A. and Shrout, T.R. 1996. Investigation of the dielectric properties of bismuth pyrochlores. *Solid State Communications* 100: 529-534.

Chaari, M., Matoussi, A. and Fakhfakh, Z. 2011. Structural and dielectric properties of sintering zinc oxide bulk ceramic. *Materials Sciences and Application* 2: 765-770.

Chen, M., Tanner, D.B. and Nino, J.C. 2005. Infrared study of the phonon modes in bismuth pyrochlores. *Physical Review B* 72: 054303.

Chen, S.Y., Lee, S.Y. and Lin, Y.J. 2003. Phase transformation, reaction kinetics and microwave characteristic of Bi_2O_3-ZnO-Nb_2O_5 ceramics. *Journal of the European Ceramic Society* 23: 873-881.

Cheng, H.F., Chen, Y.C., Liu, H.L., Hwa, L.G. and Lin, I.N. 2004. Correlation of microwave dielectric properties and crystallinity for pulsed laser deposited $Bi_2(Zn_{1/3}Nb_{2/3})O_7$ thin films. *Journal of European Ceramic Society* 24: 1791-1794.

Cheng, Z.Y., Katiyar, R.S., Yao, X. and Bhalla, A.S. 1998. Temperature dependence of the dielectric constant of relaxor ferroelectrics. *Physical Review B* 57: 8166-8177.

Chernyshev, A.P., Petrov, V.A., Titov, V.E. and Vorobyev, A.Y. 1993. Thermal radiative properties of magnesium oxide at high temperatures. *Thermochimica Acta* 218: 195-209.

Chincholkar, V.S. 1975. Structural studies on new pyrochlore compounds of type-A-3 (+) A3+ B-2 (4+) O-7 (2-). *Indian Journal of Chemistry* 13: 968-969.

Chon, M.P., Tan, K.B., Khaw, C.C., Zainal, Z., Taufiq-Yap, Y.H. and Tan, P.Y. 2012. Synthesis, structural and electrical properties of novel pyrochlores in the Bi_2O_3-CuO-Ta_2O_5 ternary system. *Ceramic International* 38: 4253-4261.

Chung, D.D.L. 2010. Dielectric behavior. In *Functional Materials: Electrical, Dielectric, Electromagnetic, Optical and Magnetic Applications*. ed. D.D.L. Chung, pp 95-200. Singapore: World Scientific Publishing Co. Pte. Ltd.

Clima, S., Pourtois, G., Hardy, A., Elshocht, S.V., Bael, M.K.V., Gendt, S.D., Wouters, D.J., Heyns, M. and Kittl, J.A. 2010. Dielectric response of Ta_2O_5, Nb_2O_5 and $NbTaO_5$ from first-principles investigations. *Journal of the Electrochemical Society* 157: G20-G25.

Cross, L.E. 1987. Relaxor ferroelectrics. *Ferroelectrics* 76: 241-267.

Cross, L.E. 1994. Relaxor ferroelectrics: an overview. *Ferroelectrics* 151: 305-320.

Djordjević, N. 2005. Influence of Bi_2O_3 on sintering and crystallization of Cordierite Ceramics. *Science of Sintering* 37: 189-197.

Du, H. and Yao, X. 2001. Investigation of dielectric properties of Bi_2O_3-ZnO-Nb_2O_5-Sb_2O_3 based pyrochlores. *Ferroelectrics* 262: 83-88.

Du, H. and Yao, X. 2002(a). Dielectric relaxation characteristics of bismuth zinc niobate pyrochlores containing titanium. *Physica B* 324: 121-126.

Du, H. and Yao, X. 2002(b). Synthesis and dielectric properties development of new thermal stable bismuth pyrochlores. *Journal of Physics and Chemistry of Solids* 63: 2123-2128.

Du, H. and Yao, X. 2002(c). Evolution of structure and dielectric properties on bismuth-based pyrochlore with TiO_2 incorporation. *Journal of Electroceramics* 9: 117-124.

Du, H. and Yao, X. 2004. Structural trends and dielectric properties of Bi-based pyrochlores. *Journal of Materials Science: Materials in Electronics* 15: 613-616.

Du, H. and Yao, X. 2005. Investigations on structural evolution and dielectric characteristics of high performance Bi-based dielectrics. *Materials Research Bulletin* 40: 1527-1535.

Du, H., Wang, H. and Yao, Xi. 2004. Observations on structural evolution and dielectric properties of oxygen-deficient pyrochlores. *Ceramics International* 30: 1383-1387.

Du, H., Yao, X. and Wang, H. 2001. The effect of CuO on sintering and dielectric properties of Bi_2O_3-ZnO-Nb_2O_5 pyrochlore. *Ferroelectrics* 262: 89-94.

Du, H., Yao, X. and Zhang, L.Y. 2002. Structure, IR spectra and dielectric properties of Bi_2O_3-ZnO-SnO_2-Nb_2O_5 quarternary pyrochlore. *Ceramics International* 28: 231-234.

Fan, H.Q. and Ke, S.M. 2009. Relaxor behaviour and electrical properties of high dielectric constant materials. *Science in China Sereis E: Technological Science* 52: 2180-2185.

Fedorov, N.F., Tunik, T.A., Razumovskij, S.N. and Mikhajlova. 1976. Iron-containing niobates of rare earths and cadmium with pyrochlore structure. *Russian Journal of Inorganic Chemistry* 21: 89-92.

Ferraro, J.R. and Nakamoto, K. 1994. Basic theory. In *Introductory Raman Spectroscopy*, ed. J.R. Ferraro and K. Nakamoto, pp 1-94. San Diego: Acedamic Press, Inc.

Fiore, R. 2000. *Circuit designer's notebook.* American Technical Ceramics.

Gao, L., Jiang, S. and Li, Y. 2012(a). Effects of growth conditions on structure and dielectric properties of bismuth-magnesium niobate thin films. *Physics Procedia* 32: 340-344.

Gao, L., Jiang, S., Li, R., Li, B. and Li, Y. 2012(b). Structure and dielectric properties of sputtered bismuth magnesium niobate thin films. *Thin Solid Films* 520: 6295-6298.

Gao, L., Jiang, S., Li, R., Li, B. and Li, Y. 2013. Influence of post deposition annealing on crystallinity and dielectric properties of bismuth magnesium niobate thin films. *Applied Surface Science* 284:523-526.

Gao, W. and Sammes, N.M. 1999. Dielectric materials. In *An Introduction to Electronic and Ionic Materials*, ed. W. Gao and N.M. Sammes, pp 148-172. Singapore: World Scientific Publishing Co. Pte. Ltd.

Glerup, M., Nielson, O.F. and Poulsen, F.W. 2001. The structural transformations from the pyrochlore structure, $A_2B_2O_7$, to the fluorite structure, AO_2, studied by raman spectroscopy and defect chemistry modelling. *Journal of Solid State Chemistry* 160: 25-32.

Ha, S., Lee, Y.S., Hong, Y.P., Lee, H.Y., Lee, Y.C., Ko, K.H., Kim, D.W., Hong, H.B. and Hong, K.S. 2003. The effect of substrate heating on the tenability of rf-sputtered Bi_2O_3-ZnO-Nb_2O_5 thin films. *Applied Physics A-Materials Science & Processing*.

Harwig, H.A. and Gerards, A.G. 1979. The polymorphism of bismuth sesquioxide. *Thermochimica Acta* 28: 121-131.

Herbert, J.M. 1985. The Properties of dielectrics. In *Ceramic Dielectrics and Capacitors*, ed. J.M. Herbert, pp 9-62. Amsterdam: Gordon and Breach Science Publishers.

Hinojosa, B.B., Nino, J.C. and Asthagiri, A. 2008. First-principles study of cubic Bi pyrochlores. *Physical Review B* 77: 104123.

Hong, Y.P., Ha, S., Lee, H.Y., Lee, Y.C., Ko, K.H., Kim, D.W., Hong, H.B. and Hong, K.S. 2002. Voltage tunable dielectric properties of rf sputtered Bi_2O_3-ZnO-Nb_2O_5 pyrochlore thin films. *Thin Solid Films* 419: 183-188.

Irvine, J.T.S., Sinclair, D.C. and West, A.R. 1990. Electroceramics: characterisation by impedance spectroscopy. *Advance Materials* 2:132-138.

Jacob, K.T., Raj, S. and Rannesh, L. 2007. Vegard's law: a fundamental relation or an approximation. *International Journal of Materials Research* 776-779.

Jonscher, A.K. 1999. Dielectric relaxation in solids. *Journal of Physics D: Applied Physics* 32: R57-R70.

Joy, P.A. 1997. Low temperature synthesis of $Mg_4Nb_2O_9$. *Materials Letters* 32: 347-349.

Kamba, S., Porokhonskyy, V., Pashkin, A., Bovtun, V. and Petzelt, J. 2002. Anomalous broad dielectric relaxation in $Bi_{1.5}Zn_{1.0}Nb_{1.5}O_7$ pyrochlore. *Physical Review B* 66: 054106.

Khan, M., Burks, D.P., Burn, I. and Schulze, W.A. 1987. Ceramic capacitor technology. In *Electronic Ceramics: Properties, Devices, and Applications.* ed. L.M. Levinson, pp 191-274. New York: Marcel Deker, Inc.

Khaw, C.C., Lee, C.K., Zainal, Z., Miles, G.C. and West, A.R. 2007. Pyrochlore phase formation in the system Bi_2O_3-ZnO-Ta_2O_5. *Journal of the American Ceramic Society* 90: 2900-2904.

Khaw, C.C., Tan, K.B. and Lee, C.K. 2009(a). High temperature dielectric properties of cubic bismuth zinc tantalate. *Ceramics International* 35: 1473-1480.

Khaw, C.C., Tan, K.B., Lee, C.K. and West, A.R. 2012. Phase equilibria and electrical properties of pyrochlore and zirconolite phases in the Bi_2O_3-ZnO-Ta_2O_5 system. *Journal of the European Ceramic Society* 32: 671-680.

Khaw, C.C., Tan, K.B., Zainal, Z. and Lee, C.K. 2009(b). Synthesis and characterisation of Cubic $Bi_3Zn_2Ta_3O_{14}$ and its related divalent-doped pyrochlore materials. *Sains Malysiana* 38: 387-393.

Kim, S.S. and Kim, W.J. 2005. Electrical properties of sol-gel derived pyrochlore-type bismuth magnesium niobate $Bi_2(Mg_{1/3}Nb_{2/3})_2O_7$ thin films. *Journal of Crystal Growth* 281: 432-439.

Kishi, H., Mizuno, Y. and Chazono, H. 2003. Base-metal electrode-multilayer ceramic capacitors: Past, Present and Future Perspectives. *Japanese Journal of Applied Physics* 42: 4-19.

Levin, I., Amos, T.G., Nino, J.C., Vanderah, T.A., Randall, C.A. and Lanagan, M.T. 2002. Structural study of an unusual cubic pyrochlore $Bi_{1.5}Zn_{0.92}Nb_{1.5}O_{6.92}$. *Journal of Solid State Chemistry* 168: 69-75.

Li, L., Xu, D., Yu, S., Dong, H., Jin, Y. and Zheng, H. 2014. Effect of substrate on the dielectric properties of bismuth magnesium niobate thin films prepared by RF magnetron sputtering. *Vacuum* 109: 21-25.

Li, L., Zhang, X., Ji, L., Ning, P. and Liao, Q. 2012. Dielectric properties and electrical behaviors of tunable $Bi_{1.5}MgNb_{1.5}O_7$ thin films. *Ceramics International* 38: 3541-3545.

Ling, C.D., Withers, R.L., Schmid, S. and Thompson, J.G. 1998. A review of bismuth-rich binary oxides in the systems Bi_2O_3-Nb_2O_5, Bi_2O_3-Ta_2O_5, Bi_2O_3-MoO_3, and Bi_2O_3-WO_3. *Journal of Solid State Chemistry* 137: 42-61.

Liu, D., Liu, Y., Huang, S.Q. and Yao, X. 1993. Phase structure and dielectric properties of Bi_2O_3-ZnO-Nb_2O_5- based dielectric ceramics. *Communications of the American Ceramic Society* 76 [8]: 2129-2132.

Liu, Y.P., Yao, X., Shen, B. and Zhang, L.Y. 2001. Synthesis, structure and dielectric properties of Bi_2O_3-ZnO-CaO-Nb_2O_5 ceramics. *Ferroelectrics* 262:65-70.

Lufaso, M.W., Vanderah, T.A., Pazos, I.M., Levin, I., Roth, R.S., Nino, J.C., Provenzano, V. and Schenck, P.K. 2006. Phase formation, crystal chemistry, and properties in the system Bi_2O_3-Fe_2O_3-Nb_2O_5. *Journal of Solid State Chemistry* 179: 3900-3910.

Lumpkin, G.R., Pruneda, M., Rios, S., Smith, K.L., Trachenko, K., Whittle, K.R. and Zaluzec, N.J. 2007. Nature of the chemical bond and prediction of radiation tolerance in pyrochlore and defect fluorite compounds. *Journal of Solid State Chemistry* 180: 1512-1518.

Macdonald, J.R. and Johnson, W.B. 2005. Fundamentals of impedance spectroscopy. In *Impedance Spectroscopy-Theory, Experiment, and Applications*, ed. E. Barsoukov and J.R. Macdonald, pp 1-26. New Jersey: Wiley-Interscience.

Mazierska, J.E., Jacob, M.V., Ledenyov, D.O. and Krupka, J. (2012). Loss tangent measurements of dielectric substrates from 15 K to 300 K with two resonators: investigation into accuracy issues. *arXiv preprint arXiv:1210.2230*.

McCauley, R.A. and Hummel, F.A. (1980). New pyrochlores of the charge-coupled type. *Journal of Solid State Chemistry* 33: 99-105.

Mergen, A. and Lee, W.E. 1997. Crystal chemistry, thermal expansion and dielectric properties of $(Bi_{1.5}Zn_{0.5})(Sb_{1.5}Zn_{0.5})O_7$ pyrochlore. *Material Research Bulletin* 32:175-189.

Mergen, A., Zorlu, H., Özdemir, M. and Yumak, M. 2011(a). Fabrication and characterisation of Cr and Co doped $Bi_{1.5}Zn_{0.92}Nb_{1.5}O_{6.92}$ pyrochlores. *Journal of the European Ceramic Society* 31: 2633-2639.

Mergen, A., Zorlu, H., Özdemir, M. and Yumak, M. 2011(b). Dielectric properties of Sm, Nd, and Fe doped $Bi_{1.5}Zn_{0.92}Nb_{1.5}O_{6.92}$ pyrochlores. *Ceramics International* 37: 37-42.

Mergen. A., Özyoldas, O. and Küçük, İ. 2012. Production and properties of In and Ir doped $Bi_{1.5}Zn_{0.92}Nb_{1.5}O_{6.92}$ pyrochlores. *Journal of the European Ceramic Society* 32: 2019-2023.

Miles, G.C. and West, A.R. 2006. Pyrochlore phases in the system ZnO-Bi_2O_3-Sb_2O_5: II. Crystal structures of $Zn_2Bi_{3.08}Sb_{2.92}O_{14+\delta}$ and $Zn_{2+x}Bi_{2.96-(x-y)}Sb_{3.04-y}O_{14.04+\delta}$. *Solid State Science* 8: 1422-1429.

Morrison, F. D., Sinclair, D.C. and West, A.R. 2001. Characterization of lanthanum-doped barium titanate ceramics using impedance spectroscopy. *Journal of the American Ceramic Society* 84: 531-538.

Moulson, A.J. and Herbert, J.M. 1990(a). Introduction. In *Electroceramics: materials· properties· applications*, ed. A.J. Moulson and J.M. Herbert, pp 1-4. London: Chapman & Hall.

Moulson, A.J. and Herbert, J.M. 1990(b). Elementary solid state science. In *Electroceramics: materials properties applications*, ed. A.J. Moulson and J.M. Herbert, pp 5-85. London: Chapman & Hall.

Moulson, A.J. and Herbert, J.M. 1990(c). Dielectrics and insulators. In *Electroceramics: materials properties applications*, ed. A.J. Moulson and J.M. Herbert, pp 182-264. London: Chapman & Hall.

Moulson, A.J. and Herbert, J.M. 1990(d). Piezoelectric ceramics. In *Electroceramics: materials properties applications*, ed. A.J. Moulson and J.M. Herbert, pp 265-317. London: Chapman & Hall.

Nenasheva, E.A. and Kartenko, N.F. 2006. Low-sintering ceramic materials based on Bi_2O_3-ZnO-Nb_2O_5 compounds. *Journal of the European Ceramic Society* 26: 1929-1932.

Nguyen, B., Liu, Y. and Withers, R.L. 2007(a). The local crystal chemistry and dielectric properties of the cubic pyrochlore phase in the $Bi_2O_3M^{2+}ONb_2O_5$ (M^{2+} = Ni^{2+} and Mg^{2+}) systems. *Journal of Solid State Chemistry* 180: 549-557.

Nguyen, H.B., Norén, L., Liu, Y., Withers, R.L., Wei, X. and Elcombe, M.M. 2007(b). The disordered structures and low temperature dielectric relaxation properties of two misplaced- displacive cubic pyrochlores found in the Bi_2O_3-M^{II}O-Nb_2O_5 (M = Mg, Ni) systems. *Journal of Solid State Chemistry* 180: 2558-2565.

Ning, P., Li, L., Zhang, Z., Wang, M. and Xia, W. 2012. Enhanced tunability of $Bi_{3/2}MNb_{3/2}O_7$ (M=Zn, Mg, Ni) thin films. *Materials Letters* 87: 5-8.

Nino, J.C., Lanagan, M.T. and Randall, M.T. 2001. Dielectric relaxation in Bi_2O_3-ZnO-Nb_2O_5 cubic pyrochlore. *Journal of Applied Physics* 89: 4512-4516.

Nino, J.C., Youn, H.J., Lanagan, M.T. and Randall, C.A. 2002. Bi_2O_3 solubility of Bi-based pyrochlores and related phases. *Journal of Materials Research* 17: 1178-1182.

Nobre, M.A.L. and Lanfredi, S. 2001. Dielectric properties of $Bi_3Zn_2Sb_3O_{14}$ ceramics at high temperature. *Materials Letters* 47: 362-366.

Nowotny, J. and Rekas, M. 1992. Dielectric ceramic materials based on alkaline earth metal titanates. In *Electronic Ceramic Materials*, ed. J. Nowotny, pp 45-143. Brookfield: Trans Tech Publications.

Osman, R.A.M. and West, A.R. 2011. Electrical characterization and equivalent circuit analysis of $(Bi_{1.5}Zn_{0.5})(Nb_{0.5}Ti_{1.5})O_7$ pyrochlore, a relaxor ceramic. *Journal of Applied Physics* 109: 074106.

Osman, R.A.M., Masó, N. and West, A.R. 2012. Bismuth zinc niobate pyrochlore, a relaxor-like non-ferroelectric. *Journal of the American Ceramic Society* 95:296-302.

Park, J.H. and Yoon, S.G. 2007. Structural and electrical properties of bismuth magnesium niobate thin films deposited at various temperatures. *Transactions on Electrical and Electronic Materials* 8:153-156.

Park, J.H., Xian, C.J., Seong, N.J., Yoon, S.G., Son, S.H., Chung, H.M., Moon, J.S., Jin, H.J., Lee, S.E., Lee, J.W., Kang, H.D., Chung, Y.K. and Oh, Y.S. 2006. Realization of a high capacitance density in $Bi_2Mg_{2/3}Nb_{4/3}O_7$ pyrochlore thin films deposited directly on polymer substrates for embedded capacitor applications. *Applied Physics Letters* 89: 232910.

Pavia, D.L., Lampman, G.M., Kriz, G.S. and Vyvyan, J.R. 2013. Infrared spectroscopy. In *Introduction to Spectroscopy, Fifth Edition*, ed. D.L. Pavia, G.M. Lampman, G.S. Kriz and J.R. Vyvyan , pp 14-106. Stamford: Cengage Learning.

Peng, D., Shen, B., Zhang, L. and Yao, X. 2004. Study on relationship between sintering atmosphere and dielectric properties for Bi_2O_3-ZnO-Ta_2O_5 system. *Ceramic International* 30: 1199-1202.

Pivovarova, A.P. 2002. Compound $Mg_2Ta_2O_7$ and its interaction with Nd_3TaO_7. *Refractories and Industrial Ceramics* 43: 172-175.

Qasrawi, A. and Mergen, A. 2012. Structural, electrical and dielectric properties of $Bi_{1.5}Zn_{0.92}Nb_{1.5-x}Ta_xO_{6.92}$ pyrochlore ceramics. *Ceramics International* 38: 581-587.

Randall, C.A., Nino, J.C., Baker, A., Youn, H.J., Hitomi, A., Thayer, R., Edge, L.F., Sogabe, T., Anderson, D., Shrout, T.R., Trolier-McKinstry, S. and Lanagan, M.T. 2003. Bi-pyrochlore and zirconolite dielectrics for intergrated passive component applications. *American Ceramic Society Bulletin* 9101-9108.

Reeve, D.A. 1969. The binary system CaO-Ta_2O_5. *Journal of the Less-Common Metals* 17: 215-222.

Ren, W., Trolier-McKinstry, S., Randall, C.A. and Shrout, T.R. 2001. Bismuth zinc niobate pyrochlore dielectric thin films for capacitive applications. *Journal of Applied Physics* 89: 767-774.

Ropp, R.C. 2012. Group 5 (V, Nb, Ta) alkaline earth compounds. In *Encyclopedia of the Alkaline Earth Compounds,* e.d. R.C. Ropp, pp 701-794. Newnes: Elsevier.

Roth, R.S. and Waring, J.L. 1962. Phase equilibrium relations in the binary system bismuth sesquioxide-niobium pentoxide. *Journal of Research of the National Bureau of Standard-A*. Physics and Chemistry 66A: 451-463.

Samara, G.A. 2003. The relaxational properties of compositionally disordered ABO_3 perovskites. *Journal of Physics: Condensed Matter* 15: R367-R411.

Sebastian, M.T. 2008(a). Measurement of microwave dielectric properties. In *Dielectric Materials for Wireless Communication*, ed. M.T. Sebastian, pp 11-48. Oxford and Amsterdam: Elsevier.

Sebastian, M.T. 2008(b). Low temperature cofired ceramics. In *Dielectric Materials for Wireless Communication*, ed. M.T. Sebastian, pp 445-512. Oxford and Amsterdam: Elsevier.

Shannon, R.D. 1976. Revised effective ionic radii and systematic studies of interatomic distances in halides and chalcogenides. *Acta Crystallography* A32: 751-767.

Shannon, R.D. 1993. Dielectric polarizabilities of ions in oxides and fluorides. *Journal of Applied Physics* 73: 348-366.

Sinclair, D.C., Morrison, F.D. and West, A.R. 2000. Applications of combined impedance and electric modulus spectroscopy to characterize electroceramics, *International Ceramics* 2: 33-38.

Singh, S., Mondal, A. K. and Krupanidhi, S.B. 2009. Fabrication and characterization of crystalline cubic bismuth zinc niobate pyrochlore ($Bi_{1.5}ZnNb_{1.5}O_7$) nanoparticles derived by sol-gel. *Advanced Science Letters* [2]: 356-359.

Sirotinkin, V.P. and Bush, A.A. 2003. Preparation and dielectric properties of $Bi_{1.5}MNb_{1.5}O_7$ (M = Cu, Mg, Mn, Ni, Zn) pyrochlore oxides. *Inorganic Materials* 39: 1130-1133.

Sleight, A.W. 1974. New ternary oxides of Re, Os, Ir and Pt with cubic crystal structures. *Materials Research Bulletin* 9: 1177-1184.

Subramanian, M.A., Aravanudan, G. and Subba Rao, G.V. 1983. Oxide pyrochlores – a review. *Progressive in Solid State Chemistry* 15: 55-143.

Sudheendran, K., Raju, K.C.J. and Jacob, M.V. 2009. Microwave dielectric properties of Ti-substituted $Bi_2(Zn_{2/3}Nb_{4/3})O_7$ pyrochlores at cryogenic temperatures. *Journal of the American Ceramic Society* 92: 1268-1271.

Sun, D., Senz, S. and Hesse, D. 2003. Topotaxial formation of $Mg_4Nb_2O_9$ and $MgNb_2O_6$ thin films on MgO (001) single crystals by vapor-solid reaction. *Journal of the American Ceramic Society* 86: 1049-1051.

Tan, K.B., Khaw, C.C., Lee, C.K., Zainal, Z. and Miles, G.C. 2010. Structures and solid solution mechanisms of pyrochlore phases in the systems Bi_2O_3-ZnO- $(Nb,Ta)_2O_5$. *Journal of Alloys Compounds* 508: 457-462.

Tan, K.B., Lee, C.K., Zainal, Z., Khaw, C.C., Tan, Y.P., Shaari, H. 2008. Reaction study and phase formation in Bi_2O_3-ZnO-Nb_2O_5 ternary system. *The Pacific Journal of Science and Technology* 9: 468-479.

Tan, K.B., Lee, C.K., Zainal, Z., Miles, G.C. and West, A.R. 2005. Stoichiometry and doping mechanism of the cubic pyrochlore phase in the system Bi_2O_3-ZnO-Nb_2O_5. *Journal of Materials Chemistry* 15: 3501-3506.

Tan, P.Y., Tan, K.B., Khaw, C.C., Zainal, Z., Chen S.K. and Chon, M.P. 2012. Structural and electrical properties of bismuth magnesium tantalate pyrochlores. *Ceramics International* 38: 5401-5409.

Tang, X.G., Chew, K.H. and Chan, H.L.W. 2004. Diffuse phase transition and dielectric tunability of $Ba(Zr_yTi_{1-y})O_3$ relaxor ferroelectric ceramics. *Acta Materialia* 52: 5177-5183.

Valant, M. and Davies, P.K. 1999. Synthesis and dielectric properties of pyrochlore solid solutions in the Bi_2O_3-ZnO-Nb_2O_5-TiO_2 system. *Journal of Materials Science* 34: 5437-5442.

Valant, M. and Davies, P.K. 2000. Crystal chemistry and dielectric properties of chemically substituted $(Bi_{1.5}Zn_{1.0}Nb_{1.5})O_7$ and $Bi_2(Zn_{2/3}Nb_{4/3})O_7$ pyrochlores. *Journal of the American Ceramic Society* 83: 147-153.

Valant, M. and Suvorov, D. 2005. The Bi_2O_3-Nb_2O_5-NiO phase diagram. *Journal of the American Ceramic Society* 88: 2540-2543.

Vandenborre, M.T. and Husson, E. 1984. Comparison of the force field in various pyrochlore families II – Phases presenting structural defects. *Journal of Solid State Chemistry* 53: 253-259.

Vanderah, T.A., Lufaso, M.W., Adler, A.U., Levin, I., Nino, J.C., Provenzano, V. and Schenck, P.K. 2006(a). Subsolidus phase equilibria and properties in the system Bi_2O_3:$Mn_2O_{3\pm x}$:Nb_2O_5. *Journal of Solid State Chemistry* 179: 3467-3477.

Vanderah, T.A., Siegrist, T., Lufaso, M.W., Yeager, M.C., Roth, R.S., Nino, J.C. and Yates, S. 2006(b). Phase formation and properties in the system Bi_2O_3:$2CoO_{1+x}$:Nb_2O_5. *European Journal of Inorganic Chemistry* 4908-4914.

Vugmeister, B.E. and Glinchuk, M.D. 1990. Dipole glass and ferroelectricity in random-site electric dipole systems. *Reviews of Modern Physics* 62: 993-1026.

Wang, H., Du, H. and Yao, X. 2003. Structural study of Bi_2O_3-ZnO-Nb_2O_5 based pyrochlores. *Materials Science and Engineering* B99: 20-24.

Wang, H., Du, H., Peng, Z., Zhang, M. and Yao, X. 2004(a). Improvements of sintering and dielectric properties on Bi_2O_3-ZnO-Nb_2O_5 pyrochlore ceramics by V_2O_5 substitution. *Ceramic International* 30:1225-1229.

Wang, H., Elsebrock, R., Schneller, T., Waser, R. and Yao, X. 2004(b). Bismuth zinc niobate ($Bi_{1.5}ZnNb_{1.5}O_7$) ceramic derived from metallo-organic decomposition precursors solution. *Solid State Communications* 132:481-486.

Wang, H., Peng, Z., Du, H.L., Yao, T. and Yao, X. 2004(c). Mn^{4+} and W^{6+} substitution on Bi_2O_3-ZnO-Nb_2O_5-based low firing ceramics. *Ceramics International* 30: 1219-1223.

Wang, H., Yao, X., Zhang, L.Y. and Xia, F. 1999. Phase transition of pyrochlore structure in Bi_2O_3-ZnO-Nb_2O_5 system. *Ferroelectrics* 229: 95-101.

Wang, Q., Wang, H. and Yao, X. 2007. Structure, dielectric and optical properties of $Bi_{1.5}ZnNb_{1.5-x}Ta_xO_7$ cubic pyrochlores. *Journal of Applied Physics* 101:104116.

Wang, X., Wang, H. and Yao, X. 1997. Structures, phase transformations and dielectric properties of pyrochlores containing bismuth. *Journal of American Society* 80: 2745-2748.

Ward, P. 1991. Multilayer ceramic capacitors materials, process and reliability. In *Electronic Ceramics*, ed. B.C.H. Steel, pp 49-66. London and New York: Elsevier Applied Science.

Wersing, W. 1991. High frequency ceramic dielectrics and their application for microwave components. In *Electronic Ceramics*, ed. B.C.H. Steel, pp 67-119. London and New York: Elsevier Applied Science.

West, A.R. 1999(a). Crystallography and diffraction techniques. In *Basic solid State Chemistry*, ed. A.R. West, pp 125-165. New York: John Wiley & Sons, Ltd.

West, A.R. 1999(b). Interpretation of phase diagram. In *Basic Solid State Chemistry*, ed. A.R. West, pp 261-292. New York: John Wiley & Sons, Ltd.

West, A.R. 1999(c). Electrical properties. In *Basic Solid State Chemistry*, ed. A.R. West, pp 293-372. New York: John Wiley & Sons, Ltd.

West, A.R., Sinclair, D.C. and Hirose, N. 1997. Characterization of electrical materials, especially ferroelectrics, by impedance spectroscopy. *Journal of Electroceramics* 1: 65-71.

Wilde, P.J. and Catlow, C.R.A. 1998. Defects and diffusion in pyrochlore structured oxides. *Solid State Ionics* 112: 173-183.

Williamson, G.K. and Hall, W.H. 1953. X-ray line broadening from filed aluminium and wolfram, *Acta Metallurgica* 1: 22-31.

Wu, M.C., Huang, Y.C. and Su, W.F. 2006(a). Silver cofirable $Bi_{1.52}Zn_{0.92}Nb_{1.5}O_{6.92}$ microwave ceramics containing CuO-based dopants. *Materials Chemistry and Physics* 100: 391-394.

Wu, M.C., Kamba, S., Bovtun, V. and Su, W.F. 2006(b). Comparison of microwave dielectric behavior between $Bi_{1.5}Zn_{0.92}Nb_{1.5}O_{6.92}$ and $Bi_{1.5}ZnNb_{1.5}O_7$. *Journal of European Ceramic Society* 26: 1889-1893.

Xian, C.J., Park, J.H., Ahn, K.C., Yoon, S.G., Lee, J.W., Kim, W.C., Lim, S.T., Sohn, S.H., Moon, J.S., Jung, H.M., Lee, S.E., Lee, I.H., Chung, Y.K., Jeon, M.K. and Woo, S.I. 2007(a). Electrical properties of $Bi_2Mg_{2/3}Nb_{4/3}O_7$ (BMN) pyrochlore thin films deposited on Pt and Cu metal at low temperatures for embedded capacitor applications. *Applied Physics Letters* 90: 052903.

Xian, C.J., Park, J.H., Yoon, S.G., Moon, J.S., Lim, S.T., Sohn, S.H., Jung, H.M., Shin, Y., Kim, W.C., Jeon, M.K. and Woo, S.I. 2007(b). Effect of thickness on electrical properties of bismuth-magnesium niobate pyrochlore thin films deposited at low temperature. *Journal of Applied Physics* 101: 084114.

Youn, H.J., Randall, C., Chen, A., Shrout, T. and Lanagan, M.T. 2002. Dielectric relaxation and microwave dielectric properties of Bi_2O_3-ZnO-Ta_2O_5 ceramics. *Journal of Materials Research* 17: 1502-1506.

Youn, H.J., Sogabe, T., Randall, C.A., Shrout, T.R. and Lanagan, M.T. 2001. Phase relations and dielectric properties in the Bi_2O_3-ZnO-Ta_2O_5 system. *Journal of the American Ceramic Society* 84: 2557-2562.

Zanetti, S.M., Pereira, M.G.S. and Nono, M.C.A. 2007. Soft-chemical derived Bi_2O_3-ZnO-Ta_2O_5 nanopowder and ceramics. *Journal of the European Ceramic Society* 27: 3647-3650.

Zanetti, S.M., Silva, D.S.A. and Thin, G.P. 2004. A chemical route for the synthesis of cubic bismuth zinc niobate pyrochlore nano-powders. *Journal of Solid State Chemistry* 177: 4546-4551.

Zhou, W. 1992. Structural chemistry and physical properties of some ternary oxides in the Bi_2O_3-Ta_2O_5 system. *Journal of Solid State Chemistry* 101: 1-17.

Zuo, W., Zuo, R. and Zhao, W. 2013. Phase transition behavior and electrical properties of lead-free $(Bi_{0.5}K_{0.5})TiO_3$-$LiNbO_3$ relaxor ferroelectric ceramics. *Ceramics International* 39: 725-730.